16th ICMGP Cape Town 2024

ICMGP 2024

CAPE TOWN • SOUTH AFRICA • 21 - 26 JULY

Using the unused data: Top-down constraints on mercury exchange from diffuse processes

Eric Roy

Aryeh Feinberg, Jenny A. Fisher, Jennifer Powell, Jason Ward, James Harnwell, Thandolwethu Dlamini, Noelle E. Selin

CSIC Consejo Superior de Investigaciones Científicas

UOW Australia

CSIRO

NSF

Model-measurement evaluations aggregate data

Gaseous elemental mercury (Hg^0)

GEOS-Chem v14.1

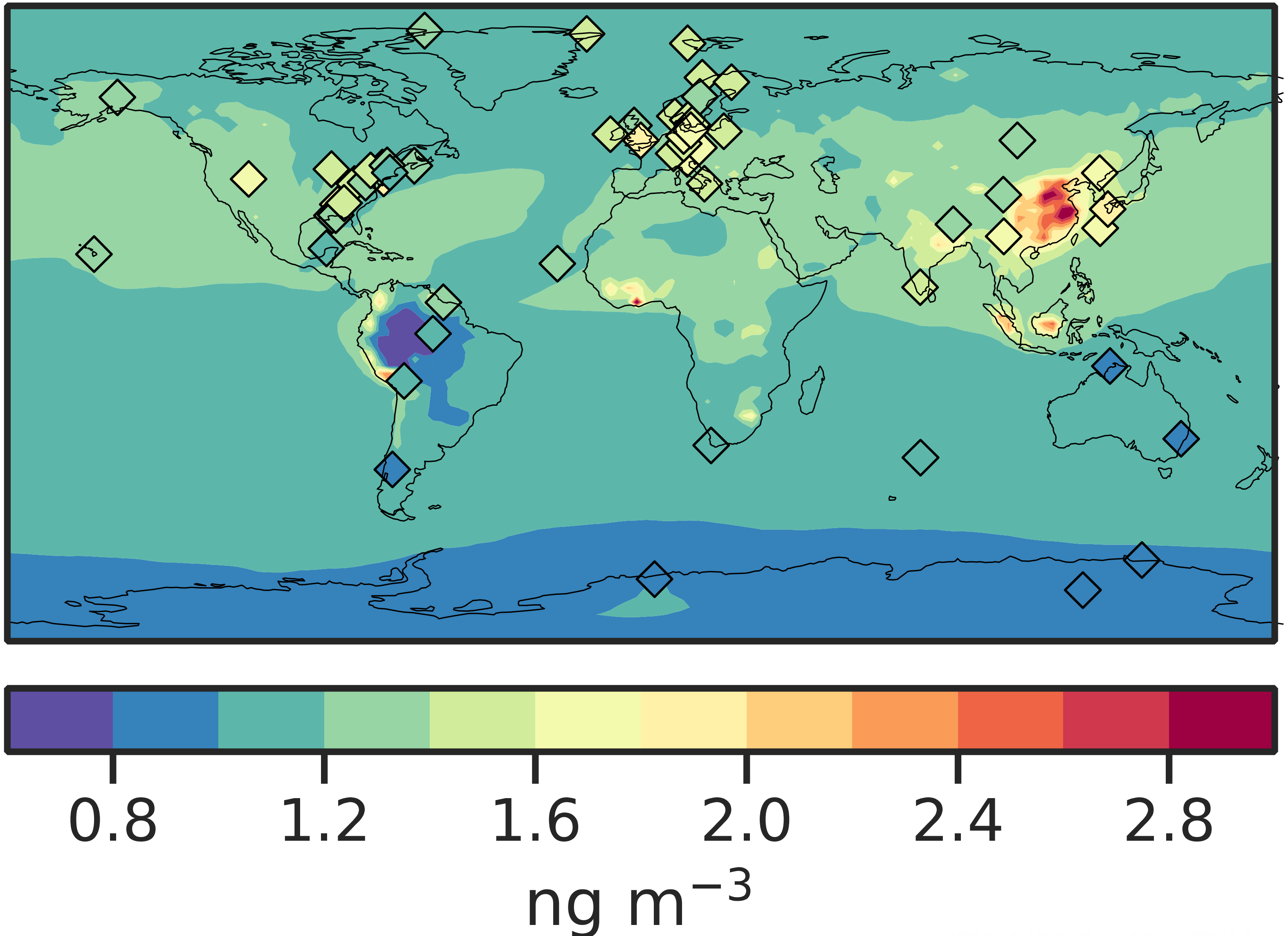

Model-measurement evaluations aggregate data

Gaseous elemental mercury (Hg^0)

GEOS-Chem v14.1

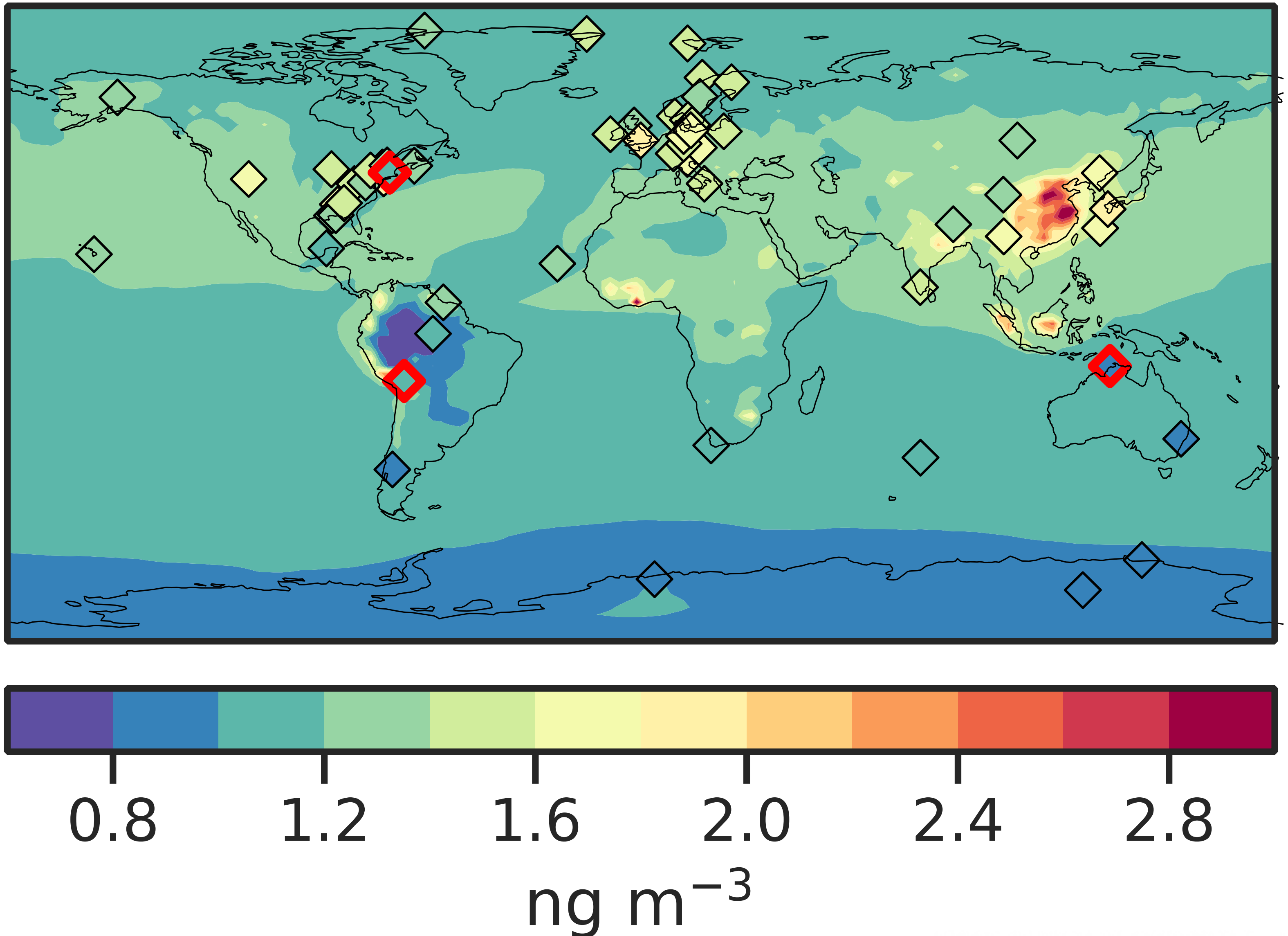

Measurement sites carry information about unique production and loss processes

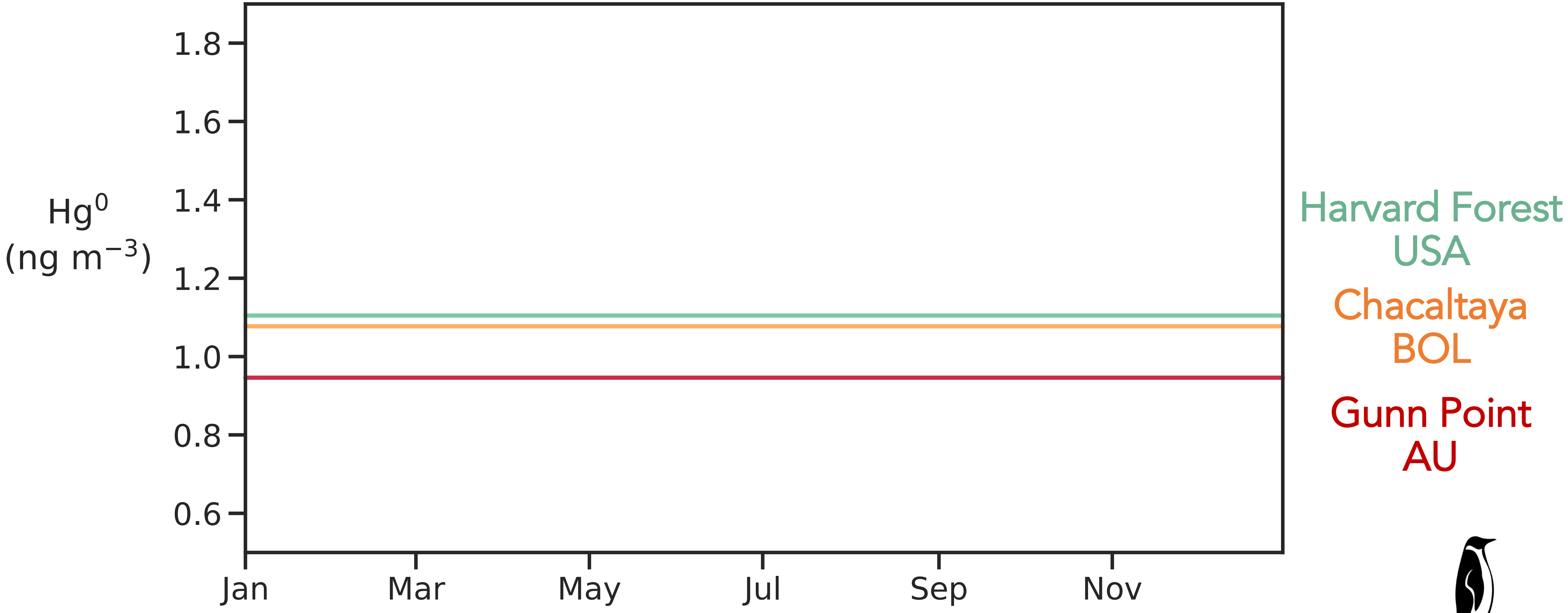

Measurement sites carry information about unique production and loss processes

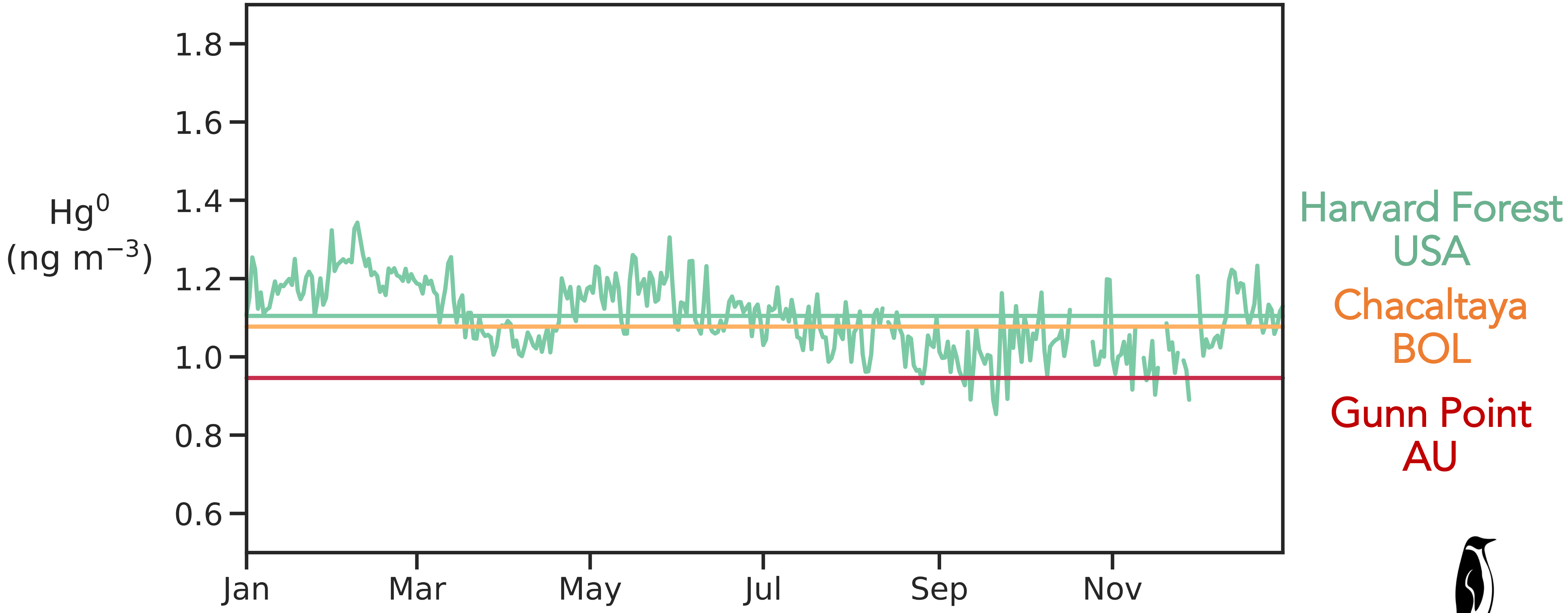

Measurement sites carry information about unique production and loss processes

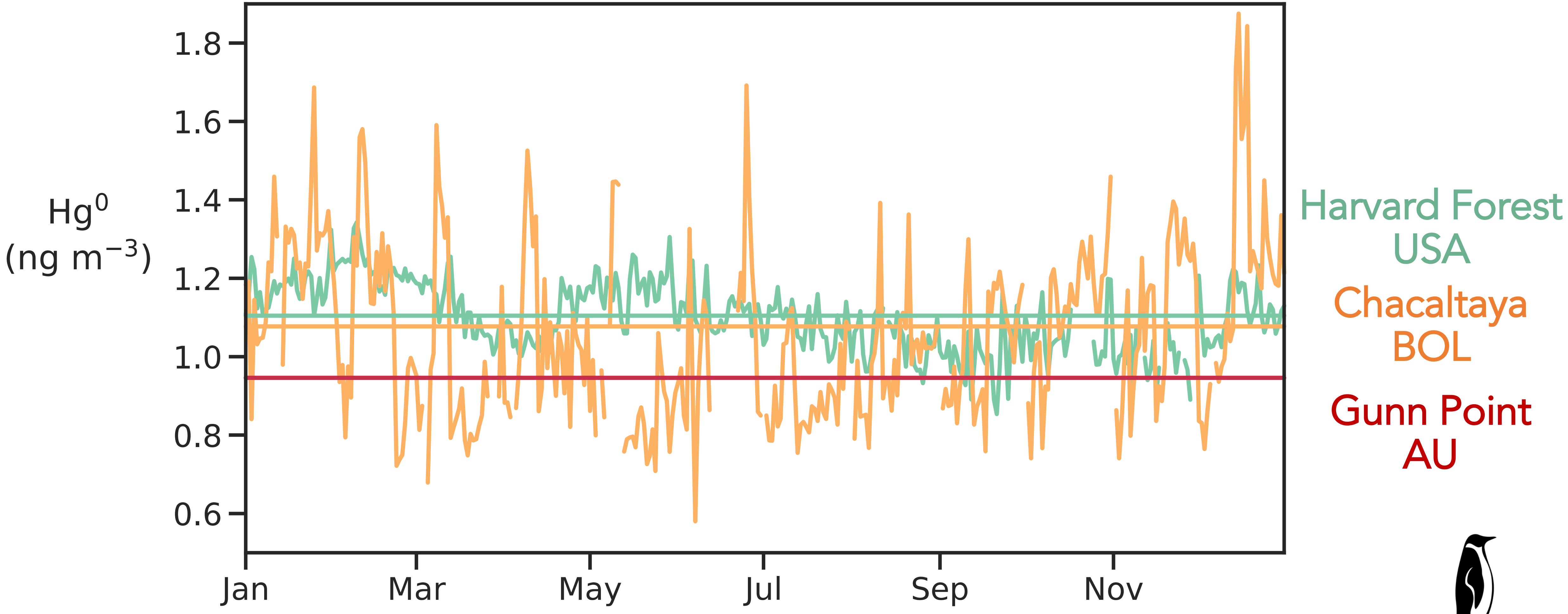

Measurement sites carry information about unique production and loss processes

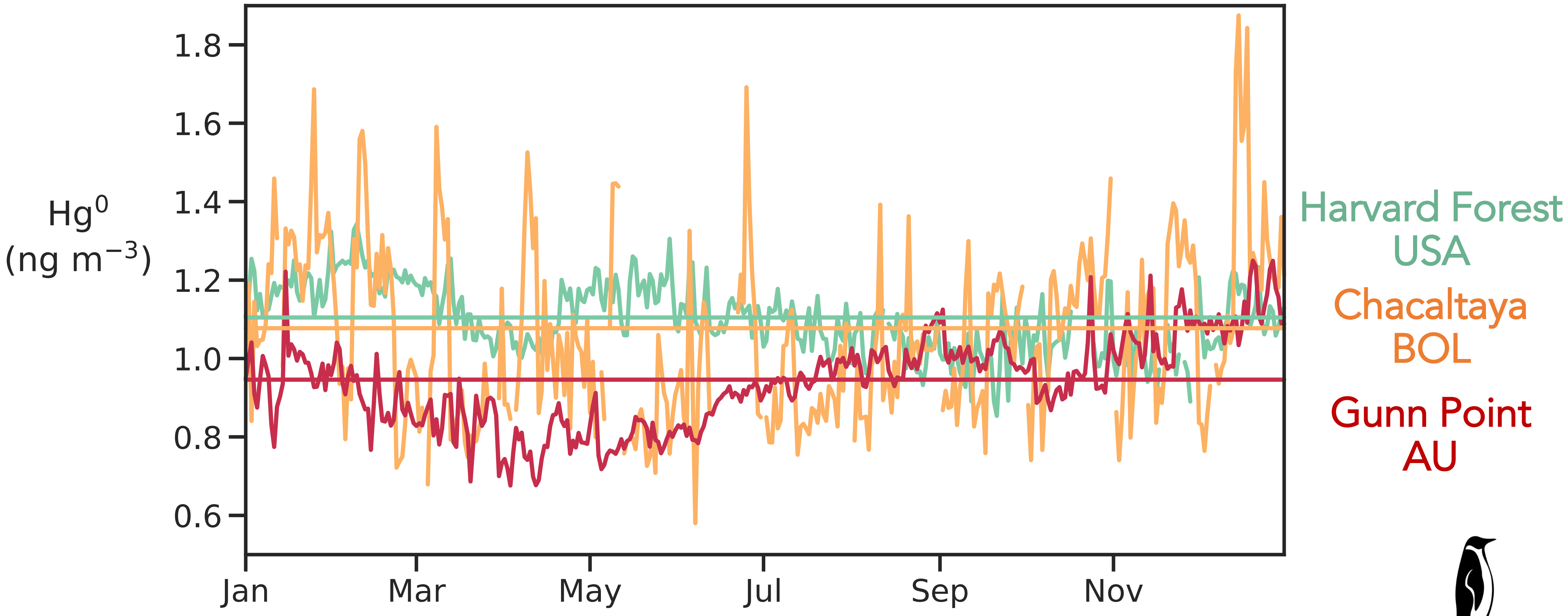

Measurement sites carry information about unique production and loss processes

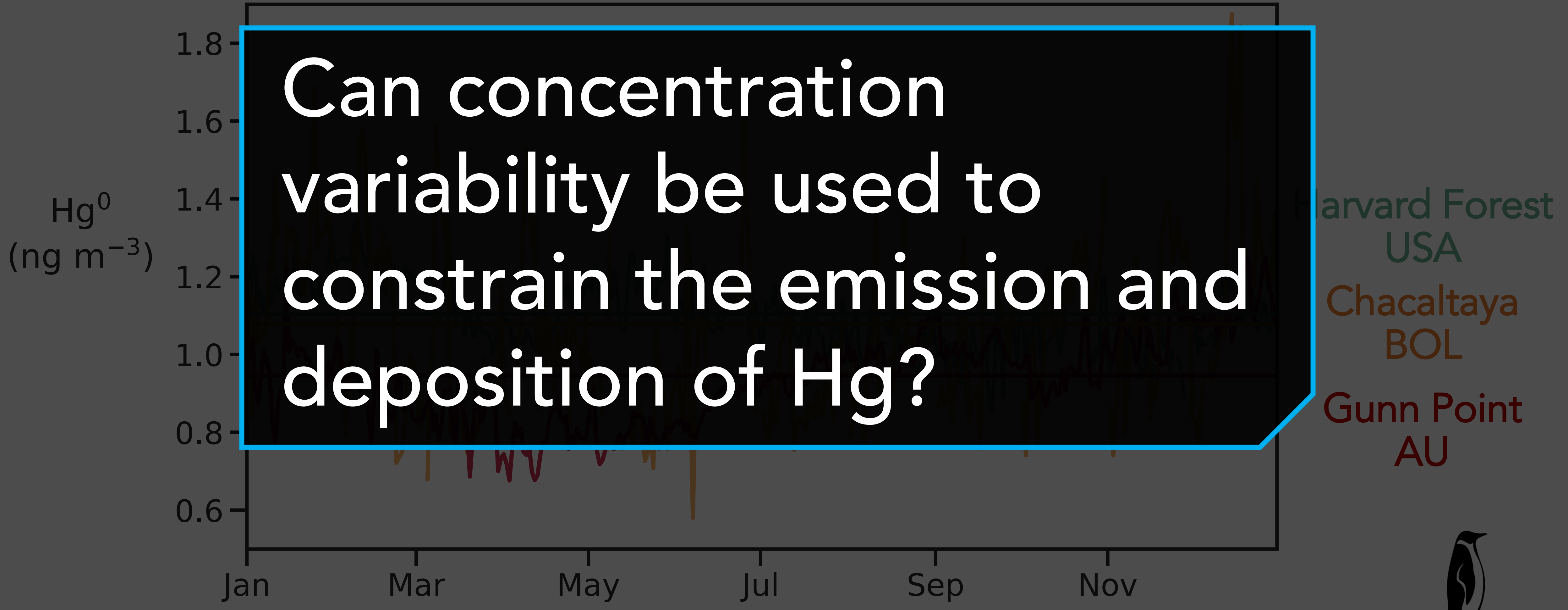

Can concentration variability be used to constrain the emission and deposition of Hg?

We select sites predominantly impacted by one surface exchange process

Dry deposition in northeastern United States

Harvard Forest, USA

Obrist et al., 2021

Artisanal and small-scale gold mining (ASGM) emissions in Peru

Chacaltaya, Bolivia

Koenig et al., 2021

Biomass burning emissions in northern Australia

Gunn Point, Australia

Howard et al., 2017

Existing dry deposition measurement at rural site offers method validation

Previously unaccounted atmospheric mercury deposition in a midlatitude deciduous forest

Daniel Obrist[a,1], Eric M. Roy[a], Jamie L. Harrison[b], Charlotte F. Kwong[c], J. William Munger[d], Hans Moosmüller[e], Christ D. Romero[a], Shiwei Sun[a,f], Jun Zhou[a], and Róisín Commane[b,c]

Results: 25 μg m^{-2} yr^{-1}

(3x greater than litterfall proxy)

Can we recover a similar insight using top-down approach?

Inverse modeling framework

Observations

Forward model

$\vec{\theta}$ = State vector

$\vec{p}$ = Parameter vector

Measurement-model error

$$\boxed{y} = \boxed{F(\vec{\theta}, \vec{p})} + \boxed{\epsilon}$$

Inverse modeling framework

Observations

Forward model

$\vec{\theta}$ = State vector

$\vec{p}$ = Parameter vector

Measurement-model error

$$\boxed{y} = \boxed{F(\vec{\theta}, \vec{p})} + \boxed{\epsilon}$$

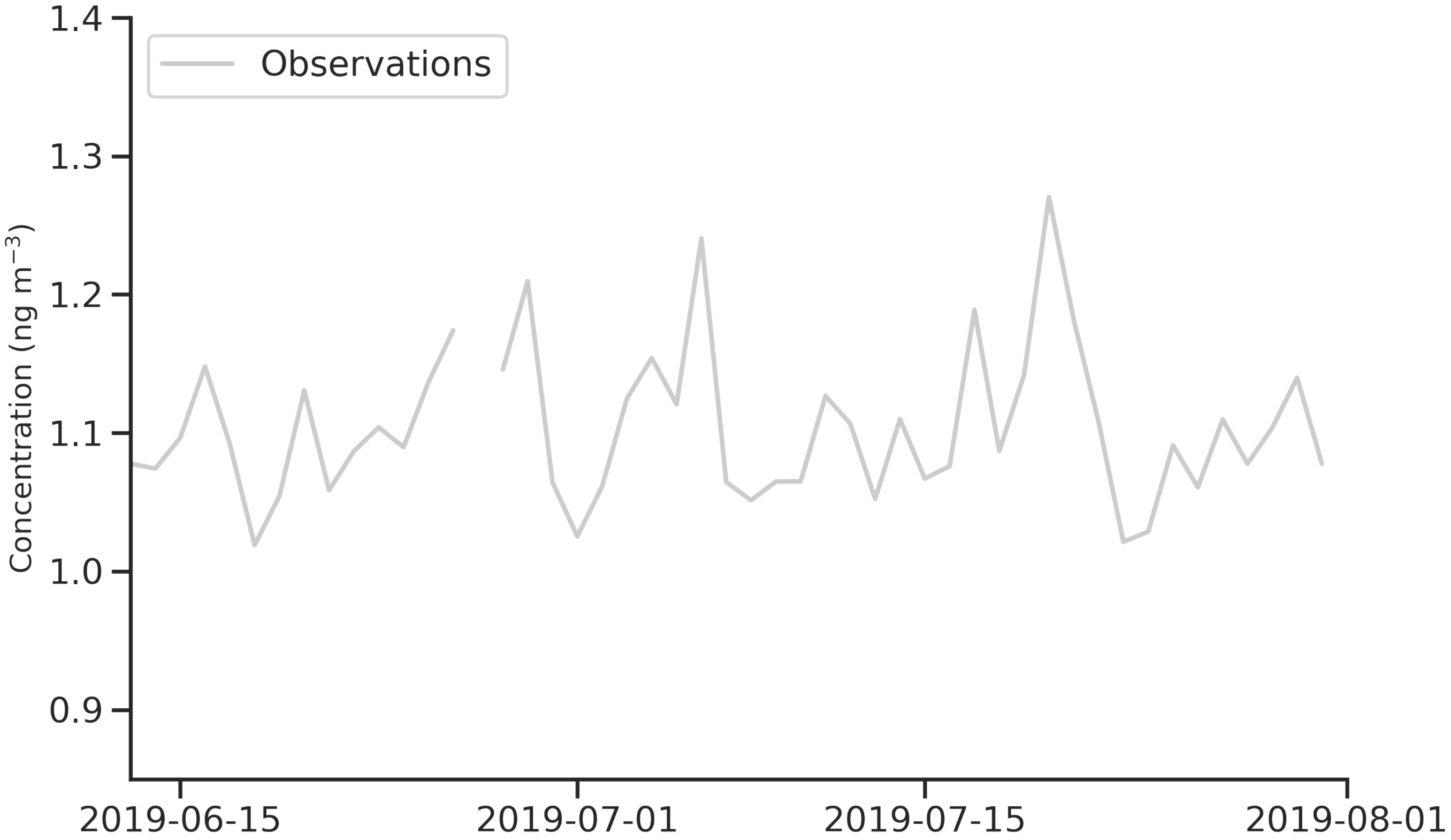

Inverse modeling framework

Observations

Forward model

$\vec{\theta}$ = State vector

$\vec{p}$ = Parameter vector

Measurement-model error

$$\boxed{y} = \boxed{F(\vec{\theta}, \vec{p})} + \boxed{\epsilon}$$

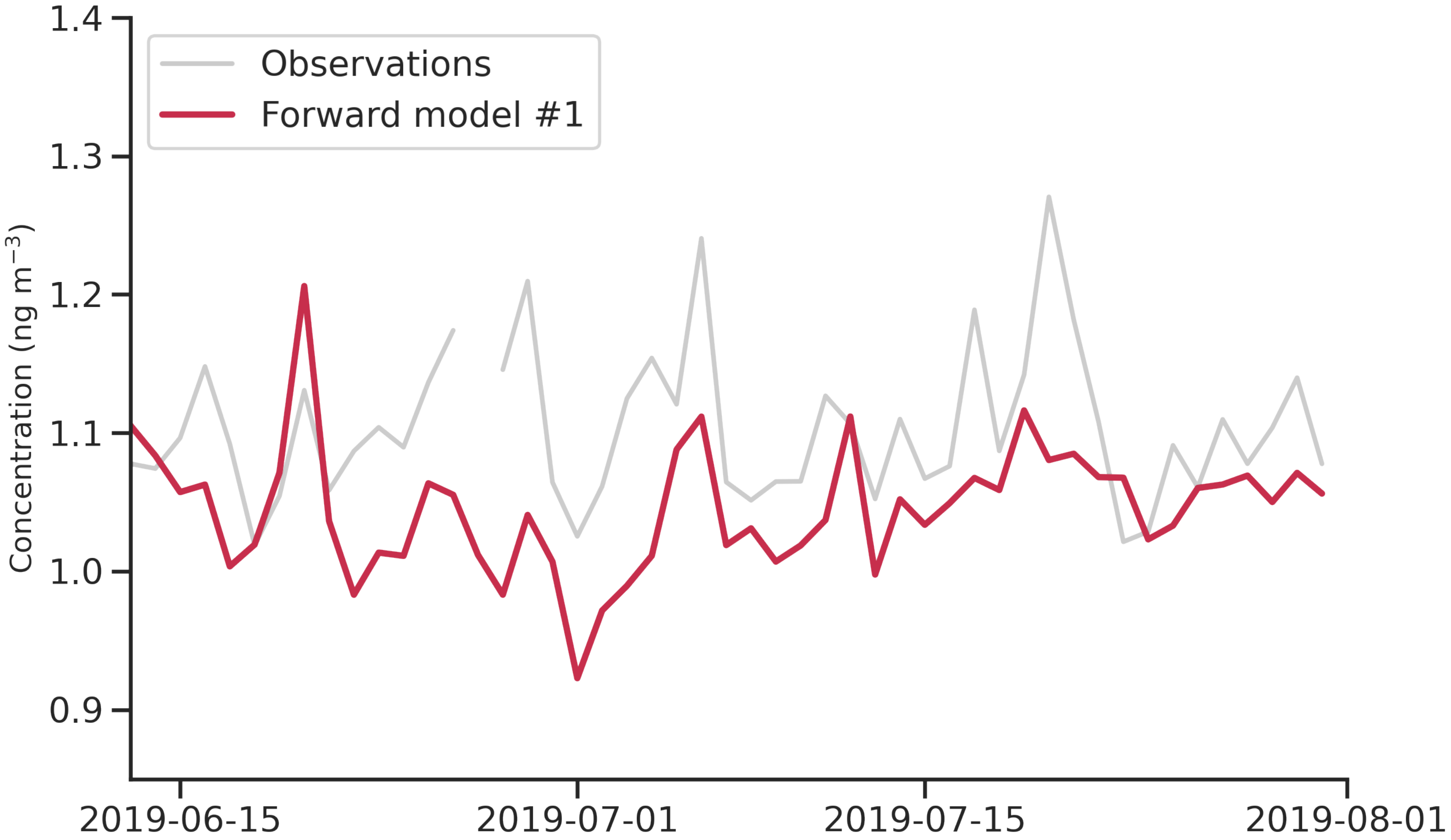

Inverse modeling framework

$$\boxed{y} = \boxed{F(\vec{\theta}, \vec{p})} + \boxed{\epsilon}$$

Observations

Forward model

$\vec{\theta}$ = State vector

$\vec{p}$ = Parameter vector

Measurement-model error

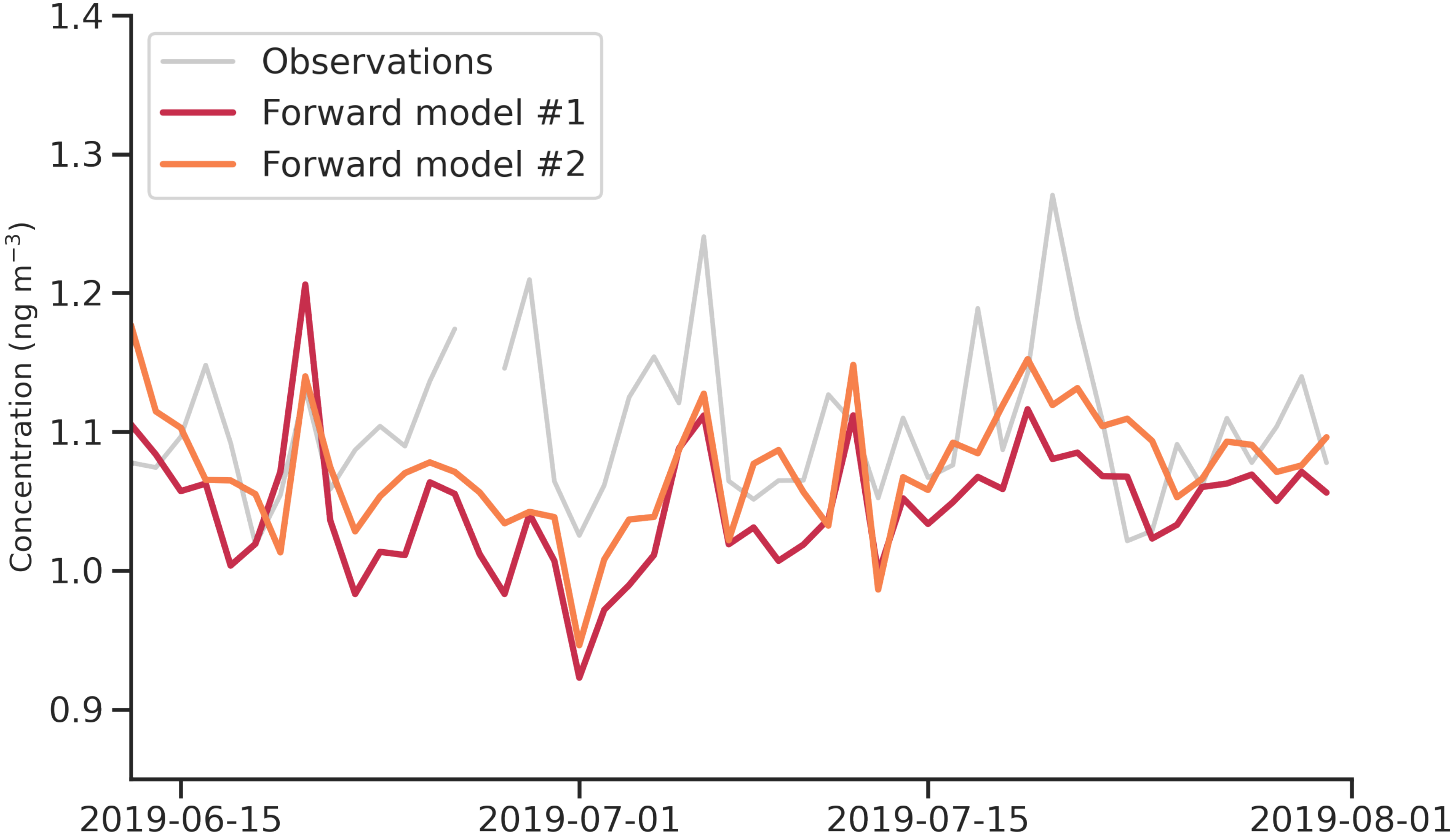

Inverse modeling framework

Observations

Forward model

$\vec{\theta}$ = State vector

$\vec{p}$ = Parameter vector

Measurement-model error

$$y = F(\vec{\theta}, \vec{p}) + \epsilon$$

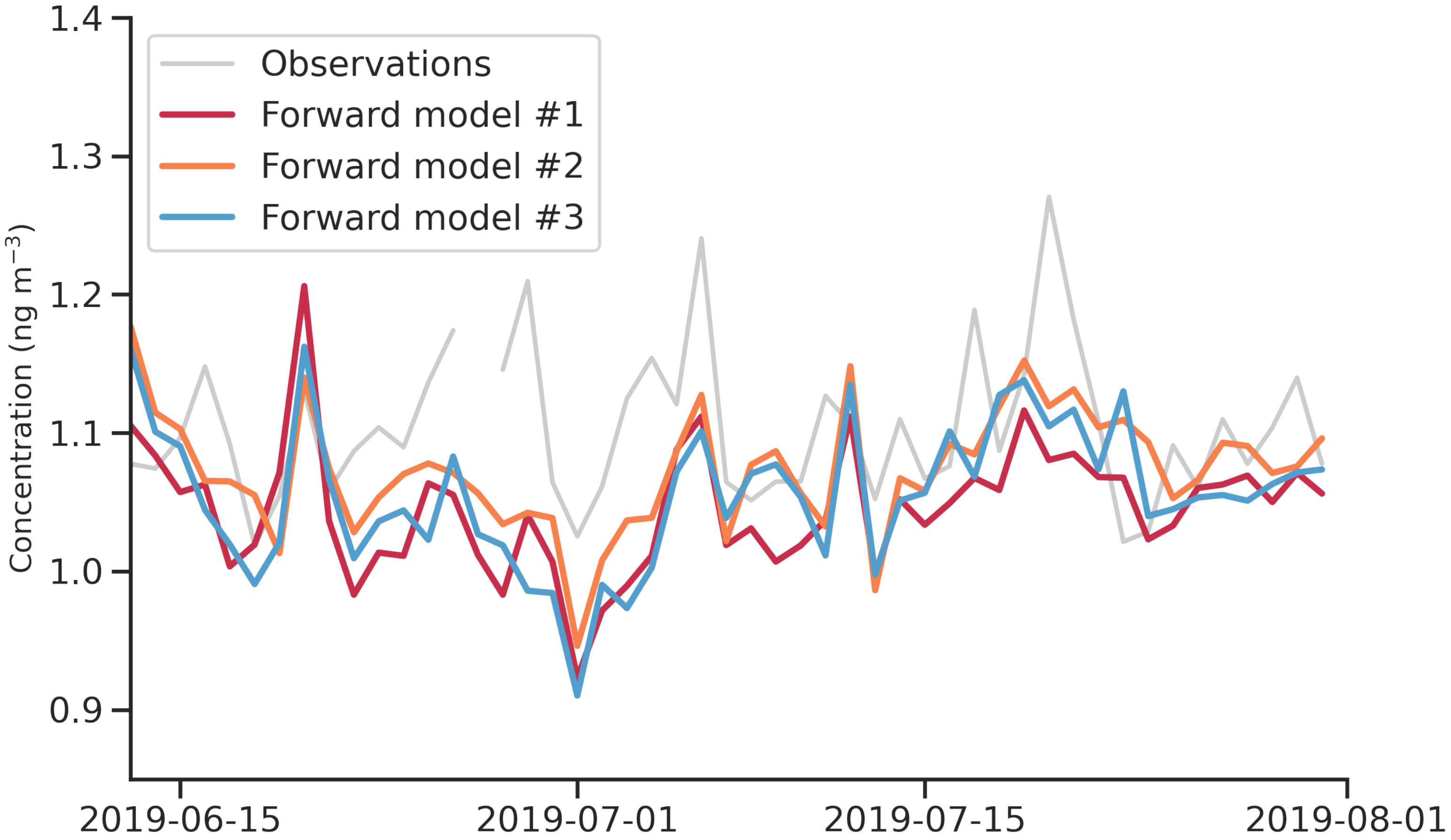

Inverse modeling framework

Observations

Forward model

$\vec{\theta}$ = State vector

$\vec{p}$ = Parameter vector

Measurement-model error

$$\boxed{y} = \boxed{F(\vec{\theta}, \vec{p})} + \boxed{\epsilon}$$

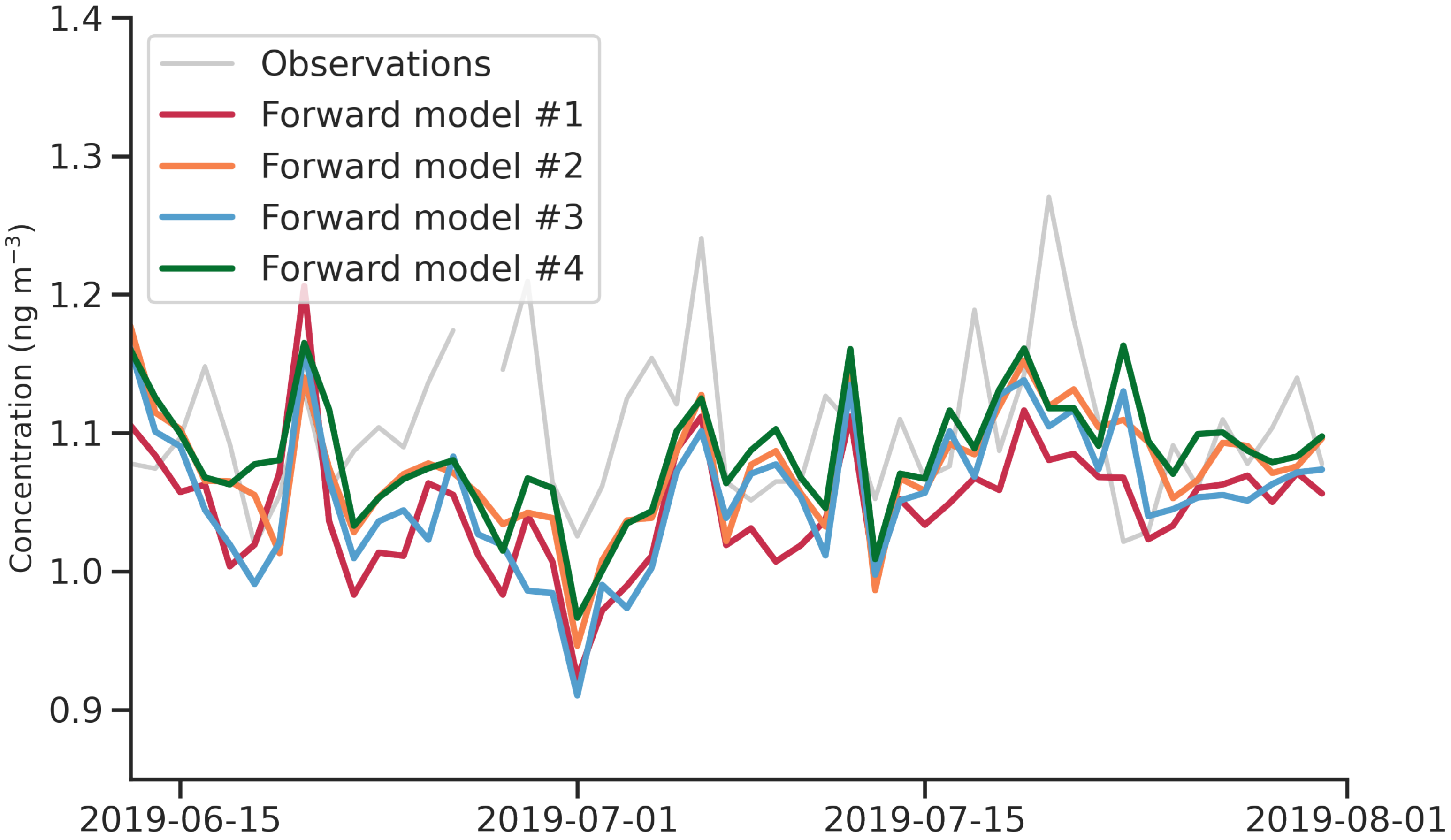

Inverse modeling framework

Observations

Forward model

$\vec{\theta}$ = State vector

$\vec{p}$ = Parameter vector

Measurement-model error

$$\boxed{y} = \boxed{F(\vec{\theta}, \vec{p})} + \boxed{\epsilon}$$

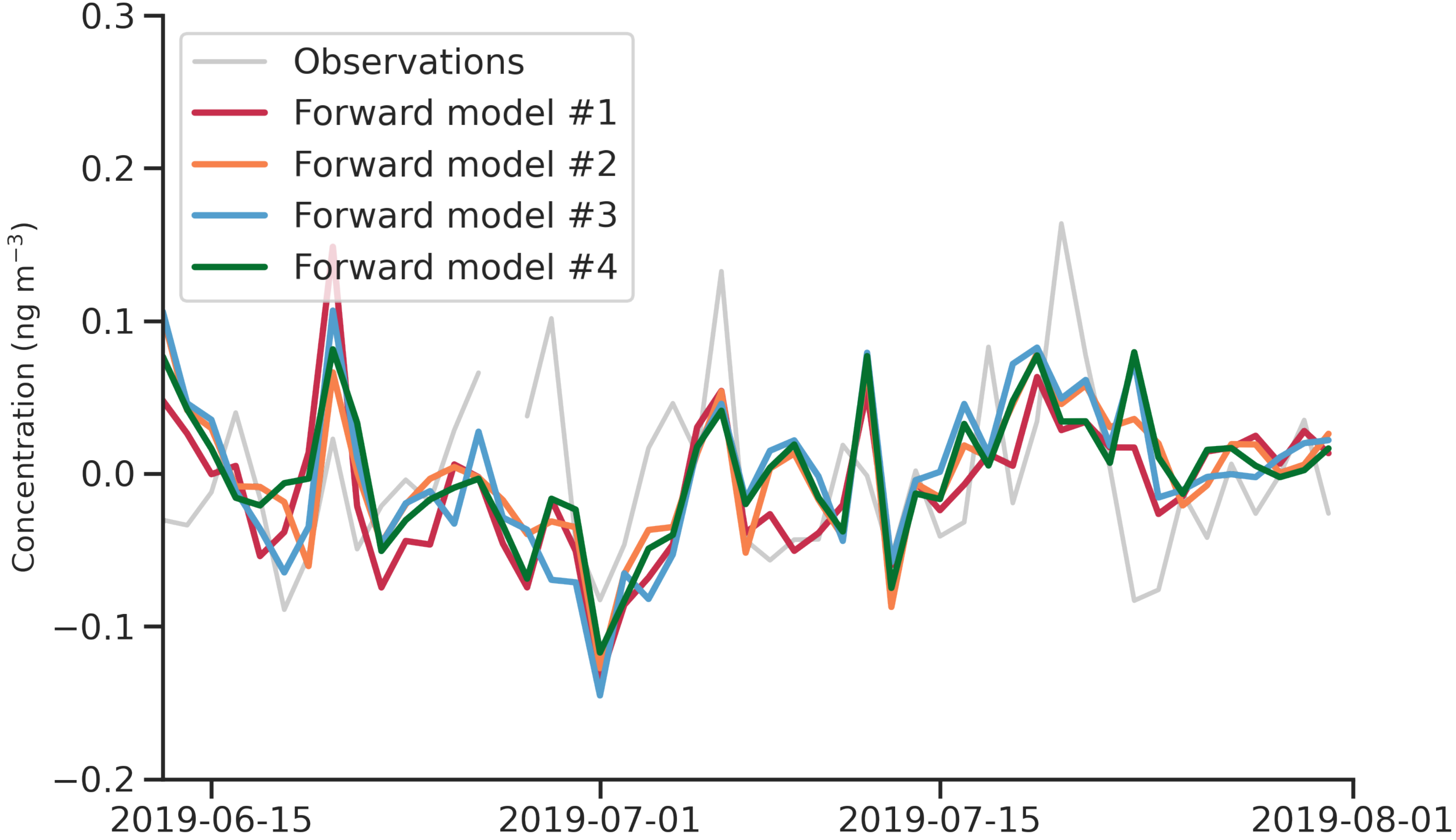

Inverse modeling framework

Observations

Forward model

$\vec{\theta}$ = State vector

$\vec{p}$ = Parameter vector

Measurement-model error:

Defined as difference in 95th percentile range

$$y = F(\vec{\theta}, \vec{p}) + \epsilon$$

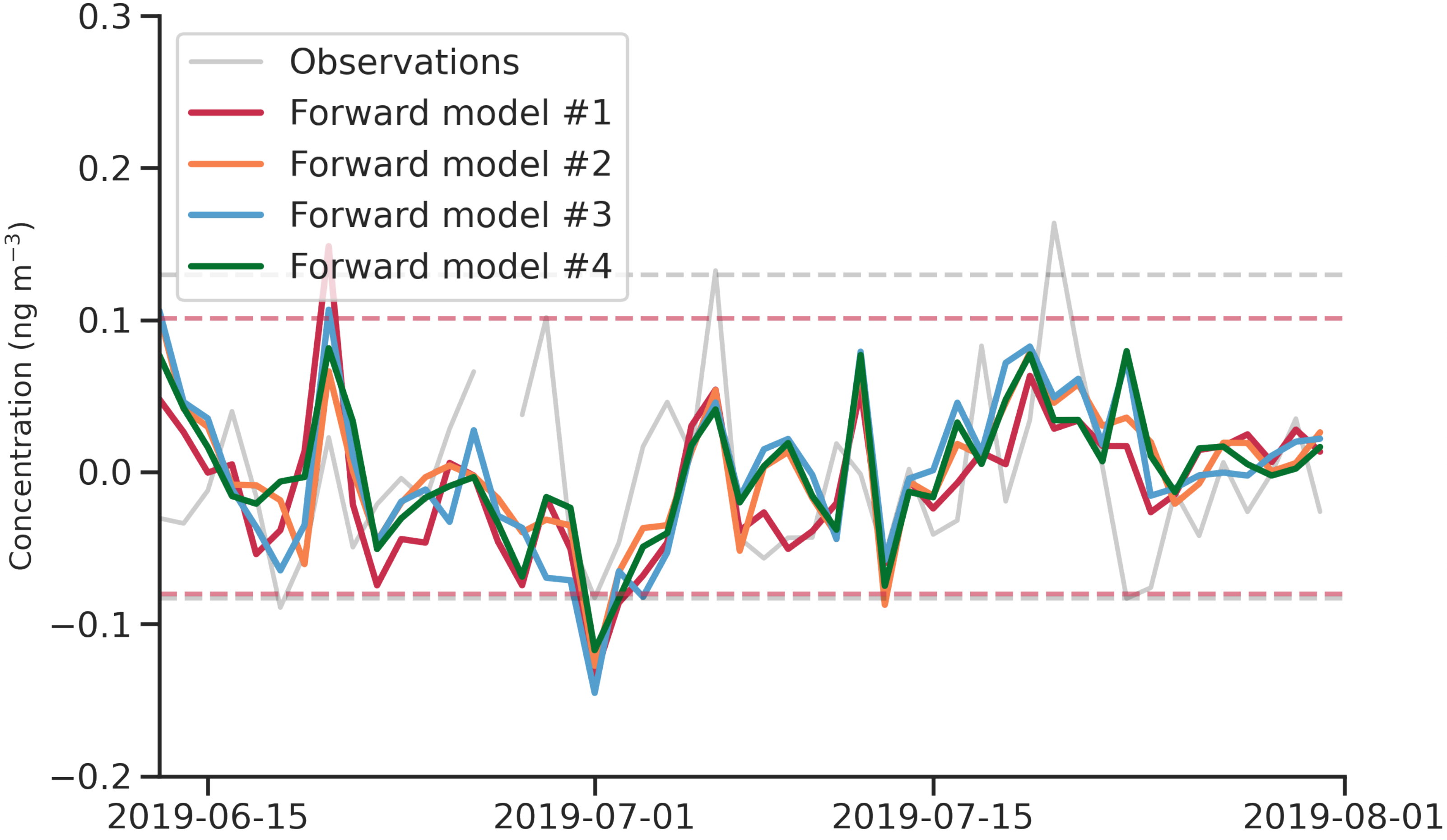

Inverse modeling framework

$$\boxed{y} = \boxed{F(\vec{\theta}, \vec{p})} + \boxed{\epsilon}$$

Observations

Forward model

$\vec{\theta}$ = State vector

$\vec{p}$ = Parameter vector

Measurement-model error:

Defined as difference in 95th percentile range

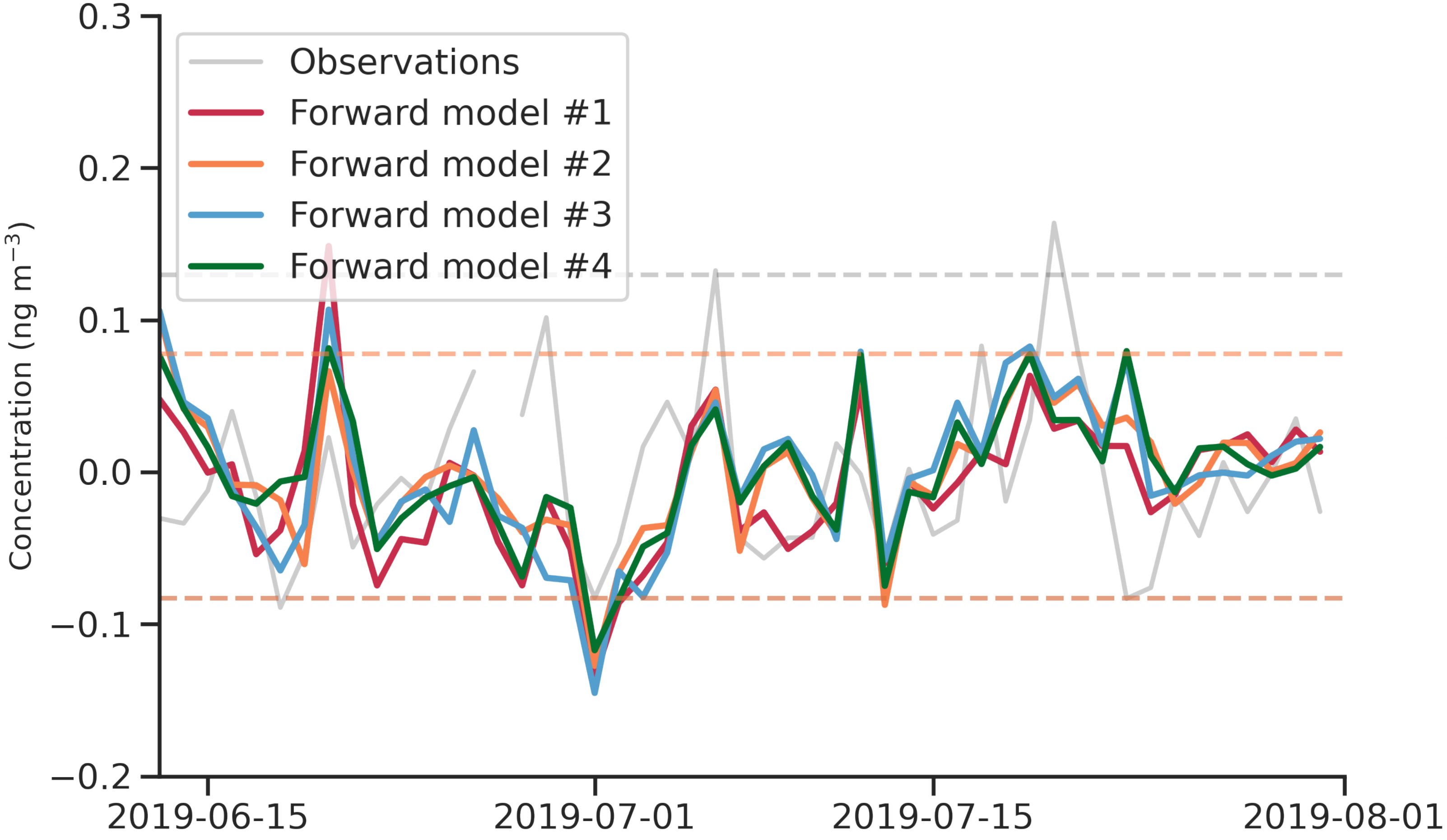

Inverse modeling framework

Observations

Forward model

$\vec{\theta}$ = State vector

$\vec{p}$ = Parameter vector

Measurement-model error:

Defined as difference in 95th percentile range

$$\boxed{y} = \boxed{F(\vec{\theta},\vec{p})} + \boxed{\epsilon}$$

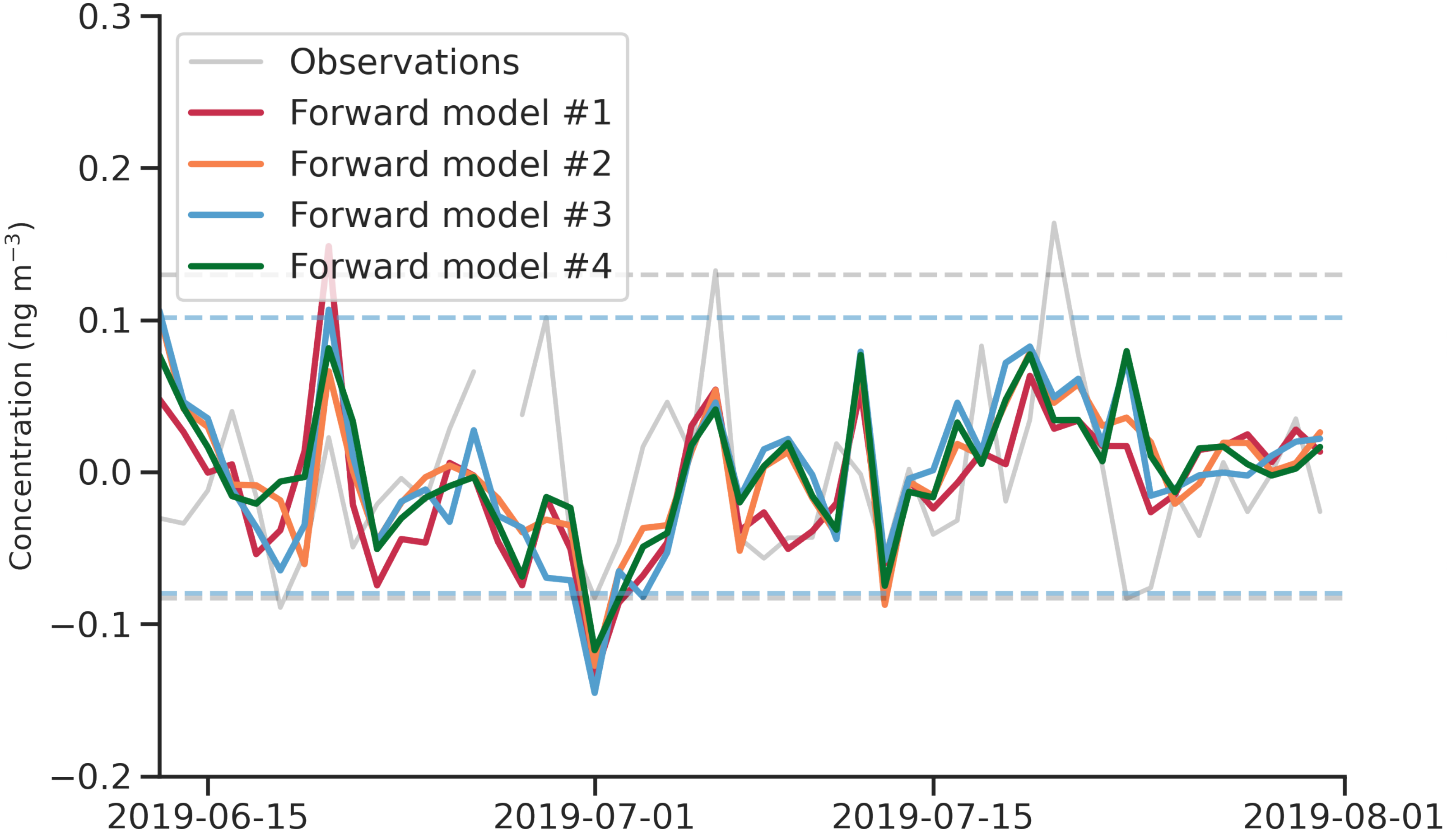

Inverse modeling framework

$$y = F(\vec{\theta}, \vec{p}) + \epsilon$$

Observations

Forward model

$\vec{\theta}$ = State vector

$\vec{p}$ = Parameter vector

Measurement-model error:

Defined as difference in 95th percentile range

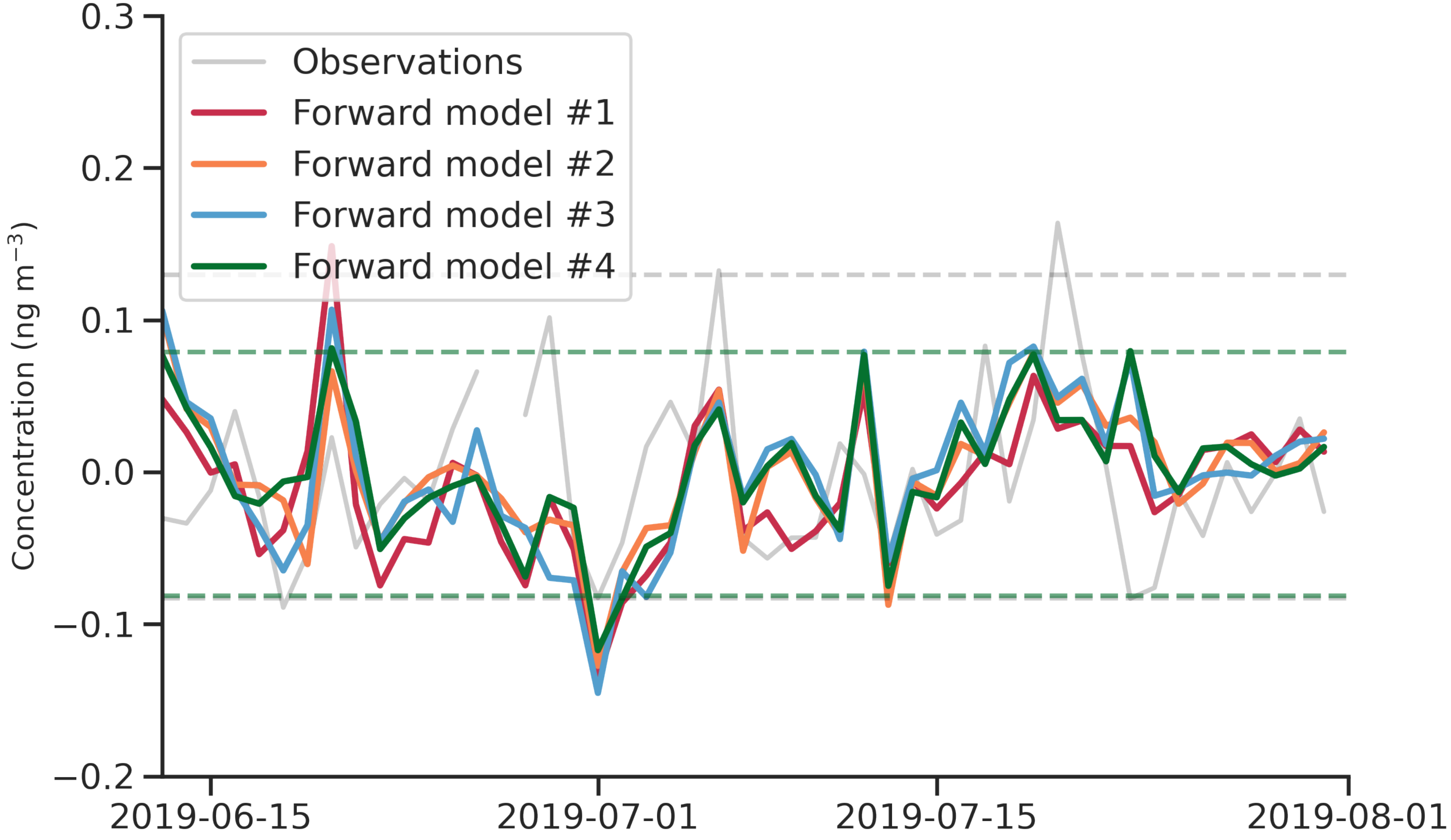

Inverse modeling framework

$$\boxed{y} = \boxed{F(\vec{\theta}, \vec{p})} + \boxed{\epsilon}$$

Observations

Forward model

$\vec{\theta}$ = State vector

$\vec{p}$ = Parameter vector

Measurement-model error:

Defined as difference in 95th percentile range

Markov-Chain Monte-Carlo sampler explores posterior distribution of $\vec{\theta}$ that minimizes ϵ while accounting for errors

Transport model uncertainty approximated using multiple models

GEOS-Chem

Global chemical transport model

- Tracks production/loss processes
- Expensive

Transport model uncertainty approximated using multiple models

GEOS-Chem

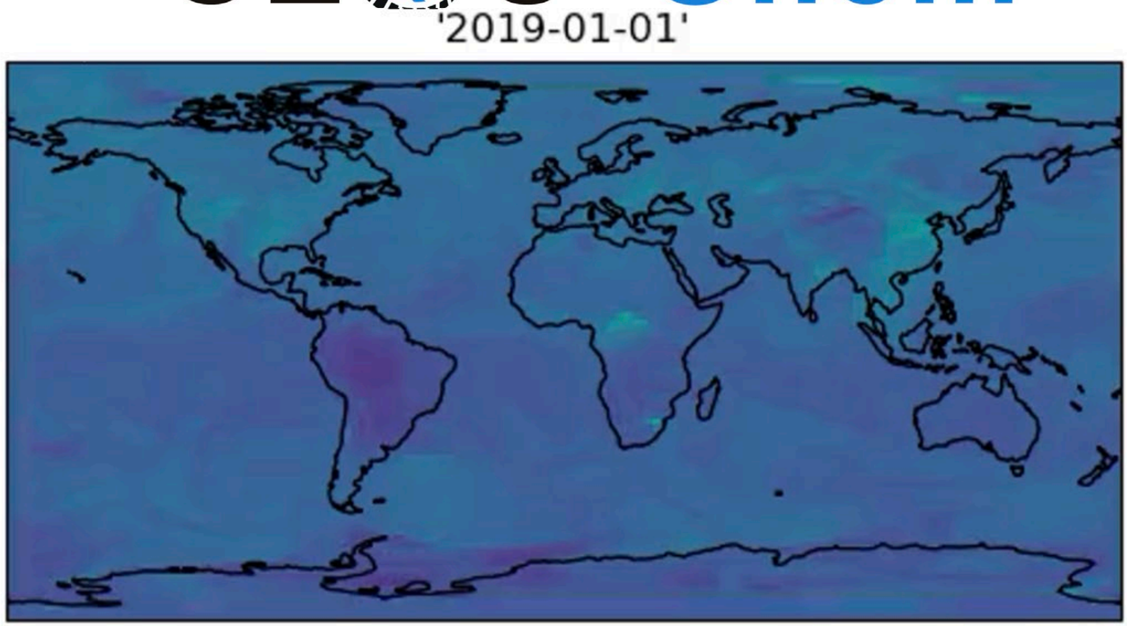

Global chemical transport model

- Tracks production/loss processes
- Expensive

STILT Model

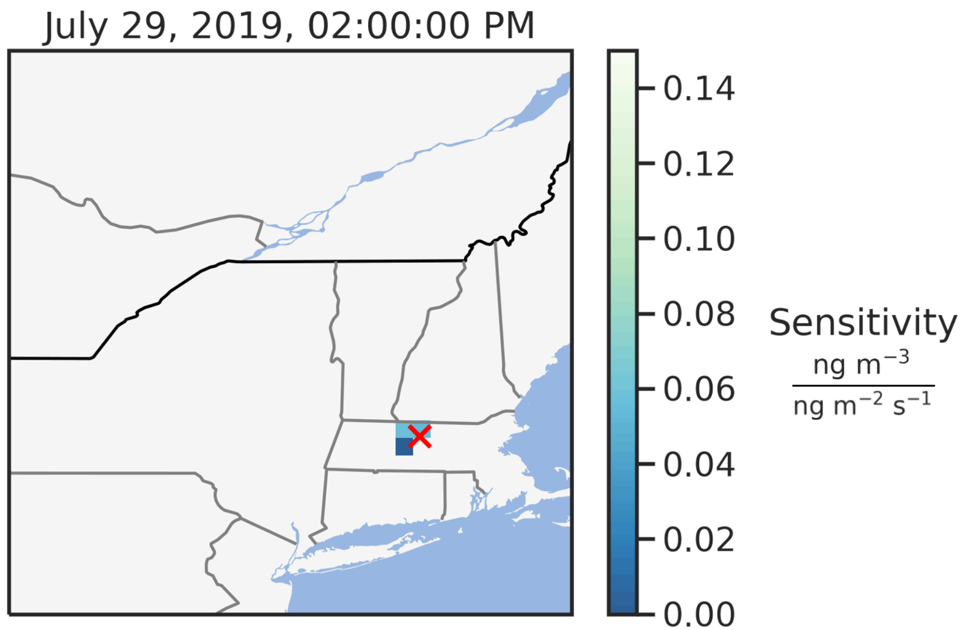

Lagrangian transport model

- Ignores other prod/loss
- Low computational cost

Dry deposition estimates at Harvard Forest

Dry deposition estimates at Harvard Forest

Dry deposition estimates at Harvard Forest

Dry deposition estimates at Harvard Forest

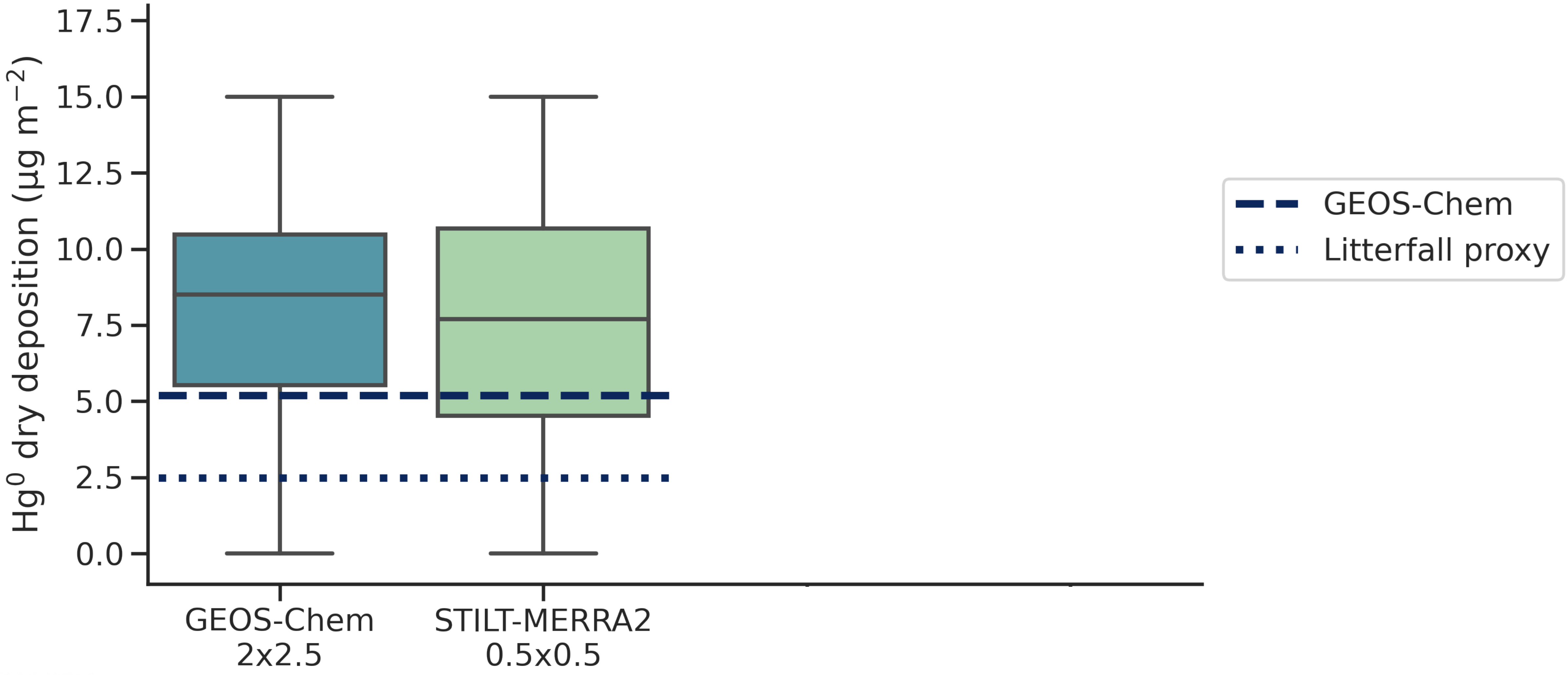

Dry deposition estimates at Harvard Forest

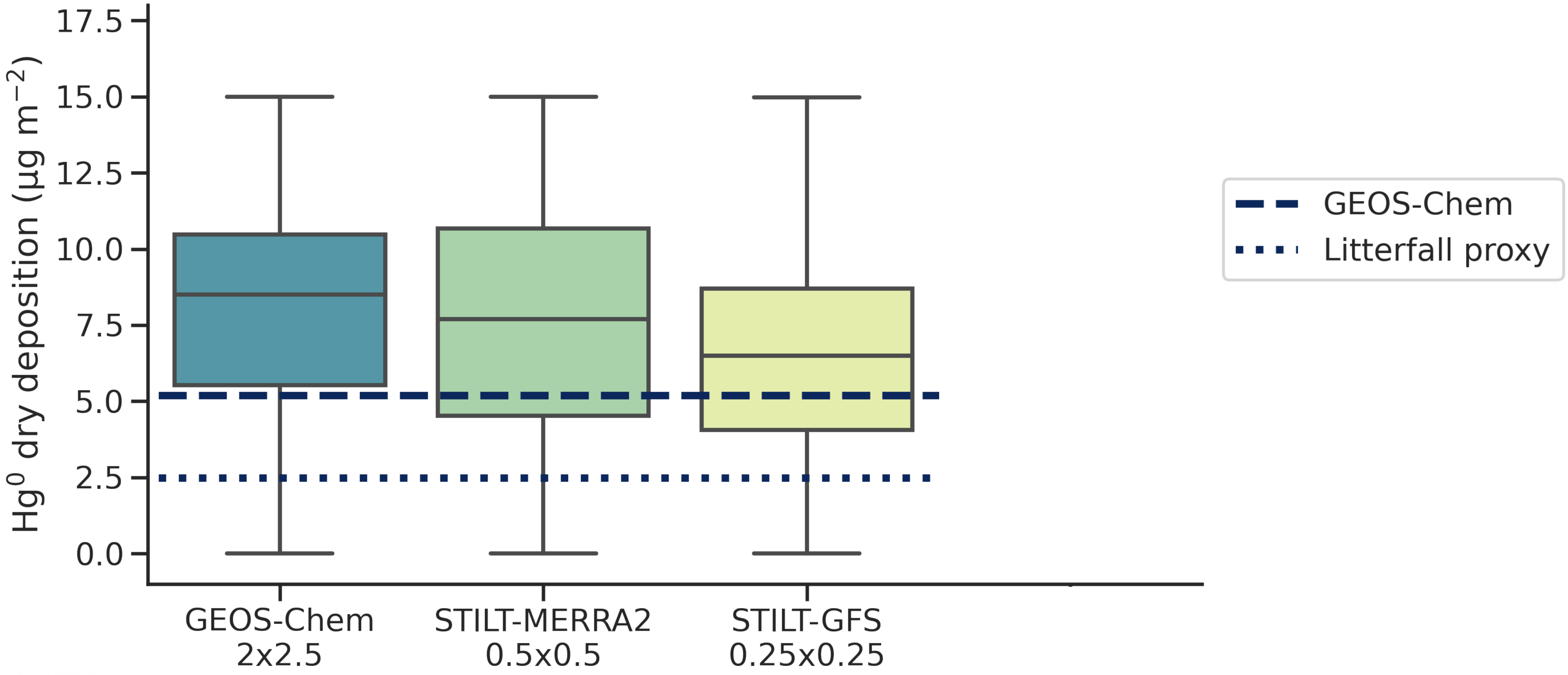

Dry deposition estimates at Harvard Forest

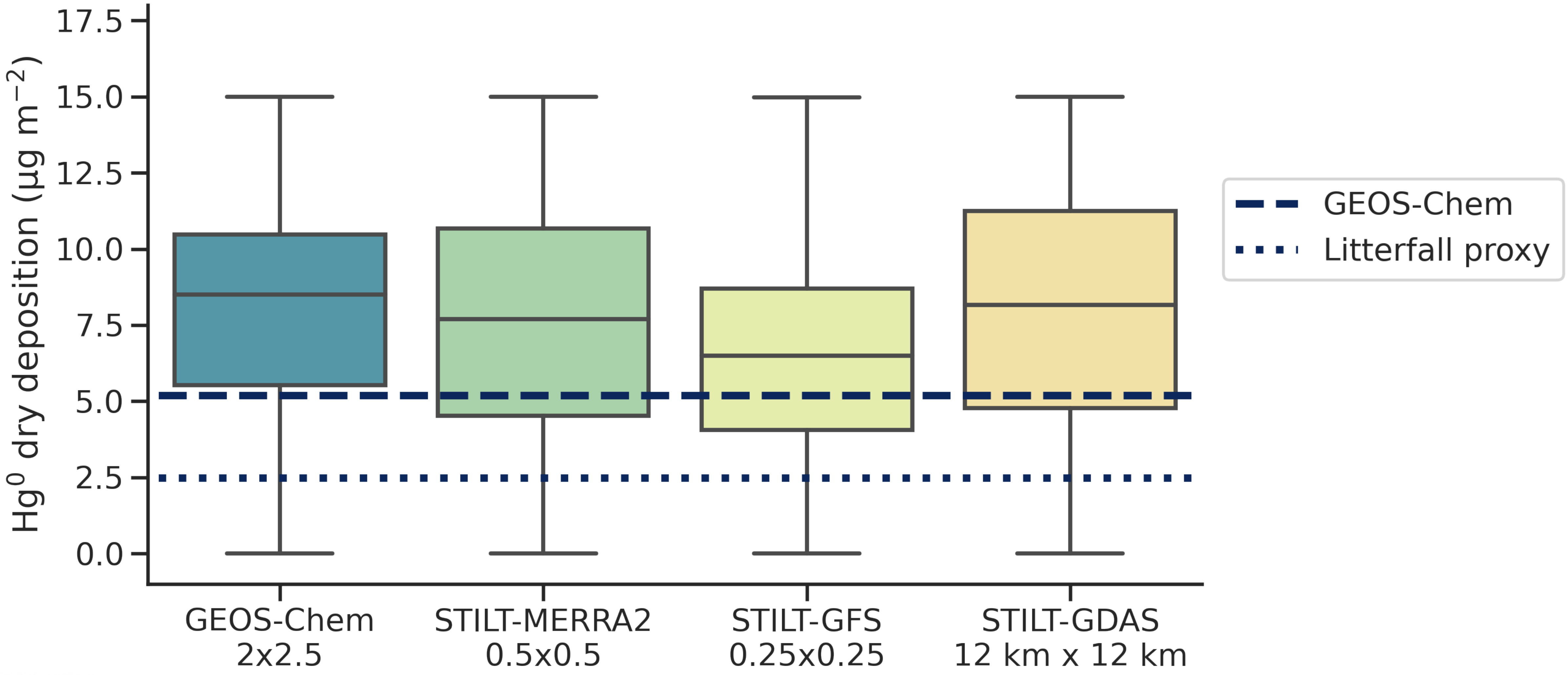

Dry deposition estimates at Harvard Forest

All distributions lie above litterfall-based proxies

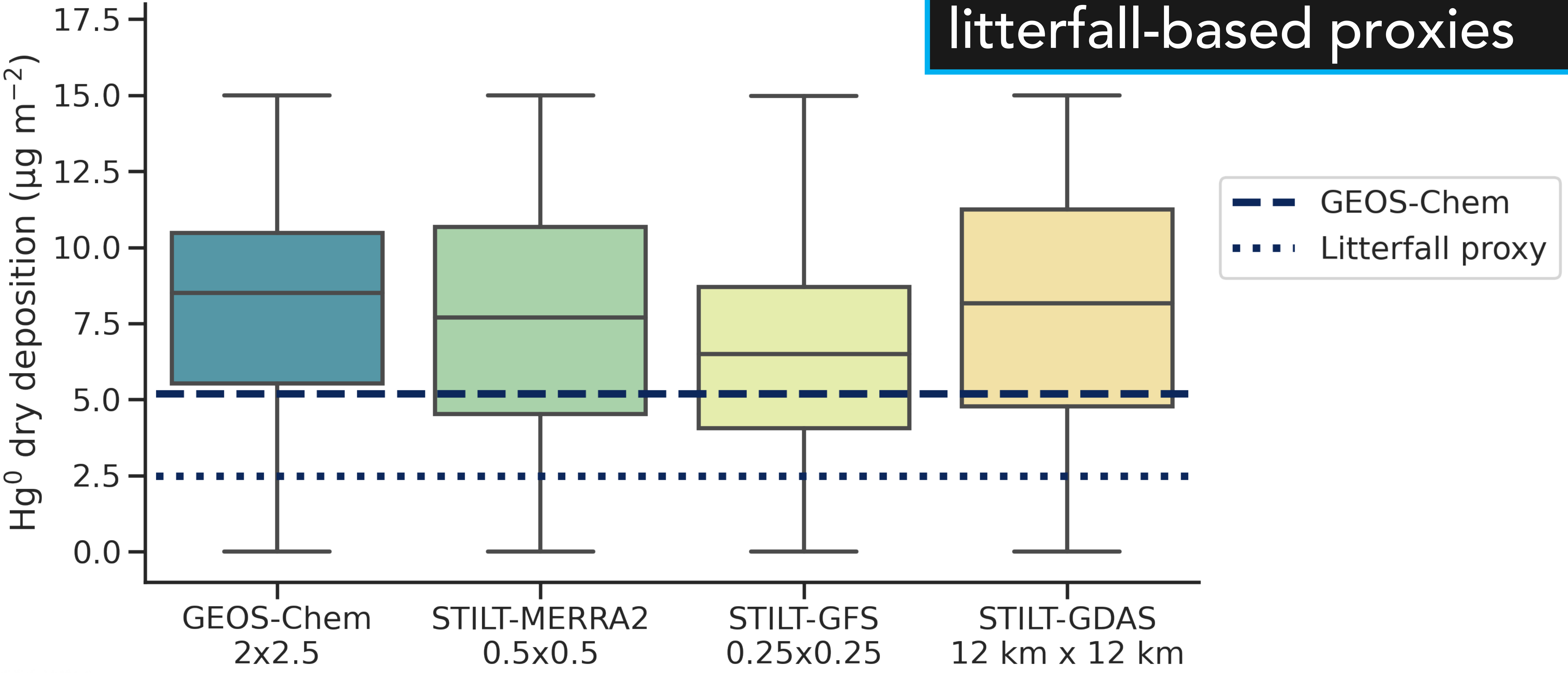

Dry deposition estimates at Harvard Forest

All distributions lie above litterfall-based proxies

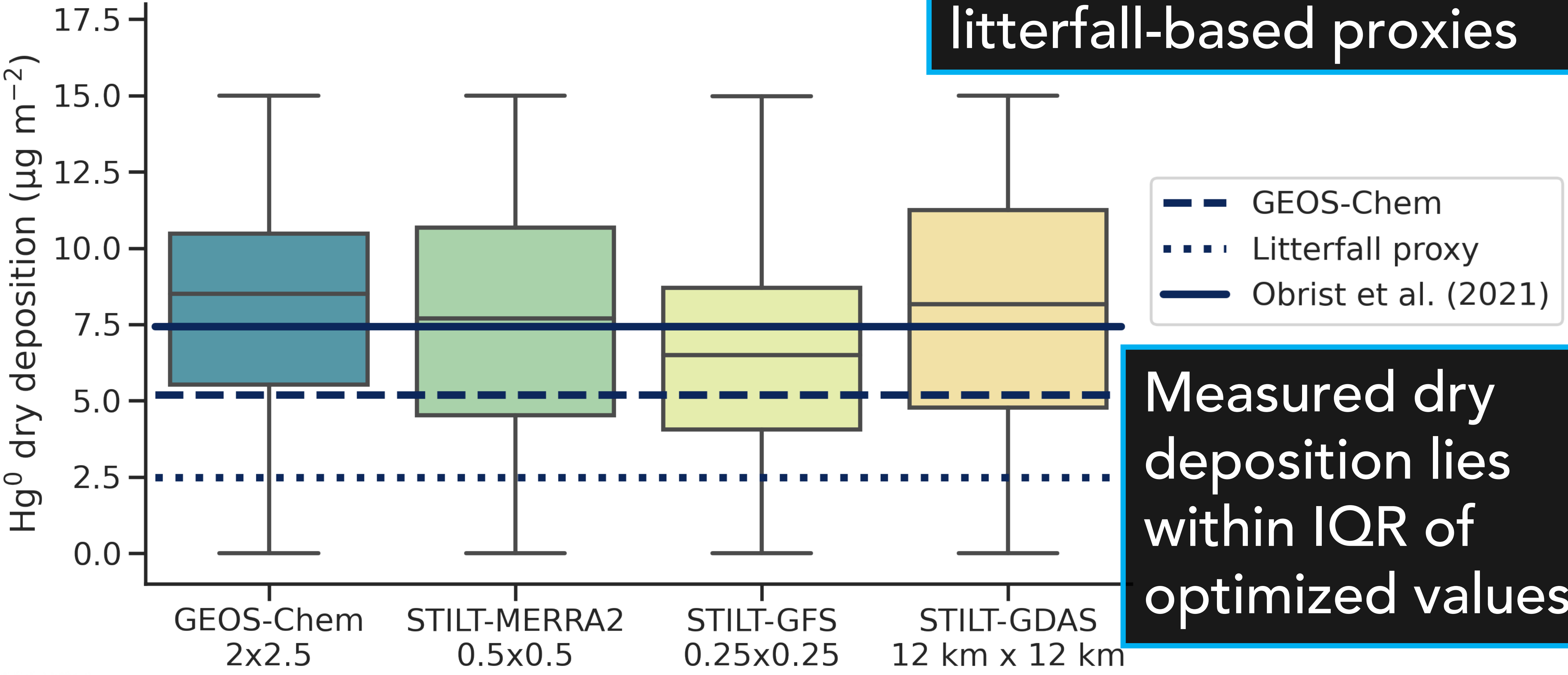

Measured dry deposition lies within IQR of optimized values!

Mountaintop Hg^0 concentration record impacted by poorly constrained ASGM emissions
(Koenig et al., 2021)

Madre de Dios

Mountaintop Hg^0 concentration record impacted by poorly constrained ASGM emissions
(Koenig et al., 2021)

Madre de Dios

Global Mercury Assessment (2018) 1.3 Mg yr^{-1}

Emissions identified by Dlamini (2022)

Mountaintop Hg^0 concentration record impacted by poorly constrained ASGM emissions (Koenig et al., 2021)

Madre de Dios

Global Mercury Assessment (2018)	1.3 Mg yr^{-1}
Artisanal Gold Council	55 Mg yr^{-1}

Emissions identified by Dlamini (2022)

Optimized emissions in Madre de Dios

Optimized emissions in Madre de Dios

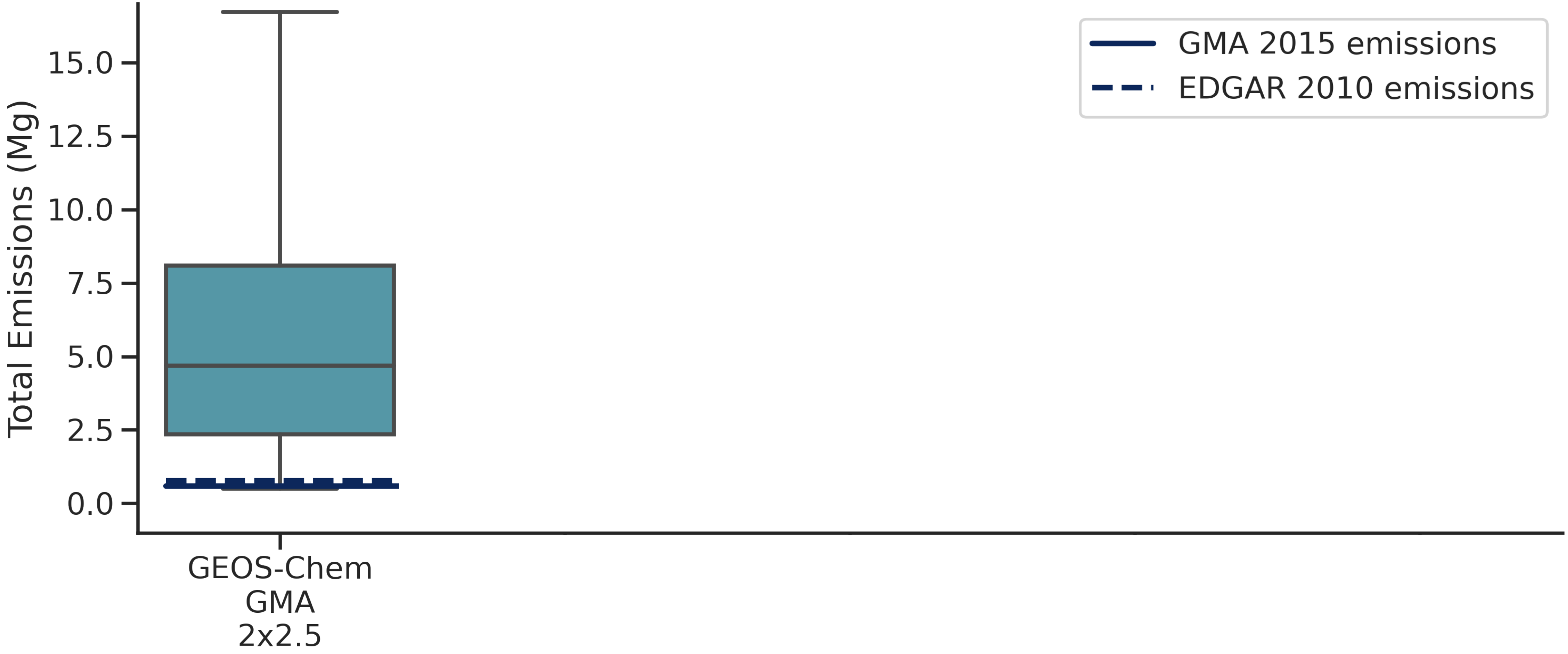

Optimized emissions in Madre de Dios

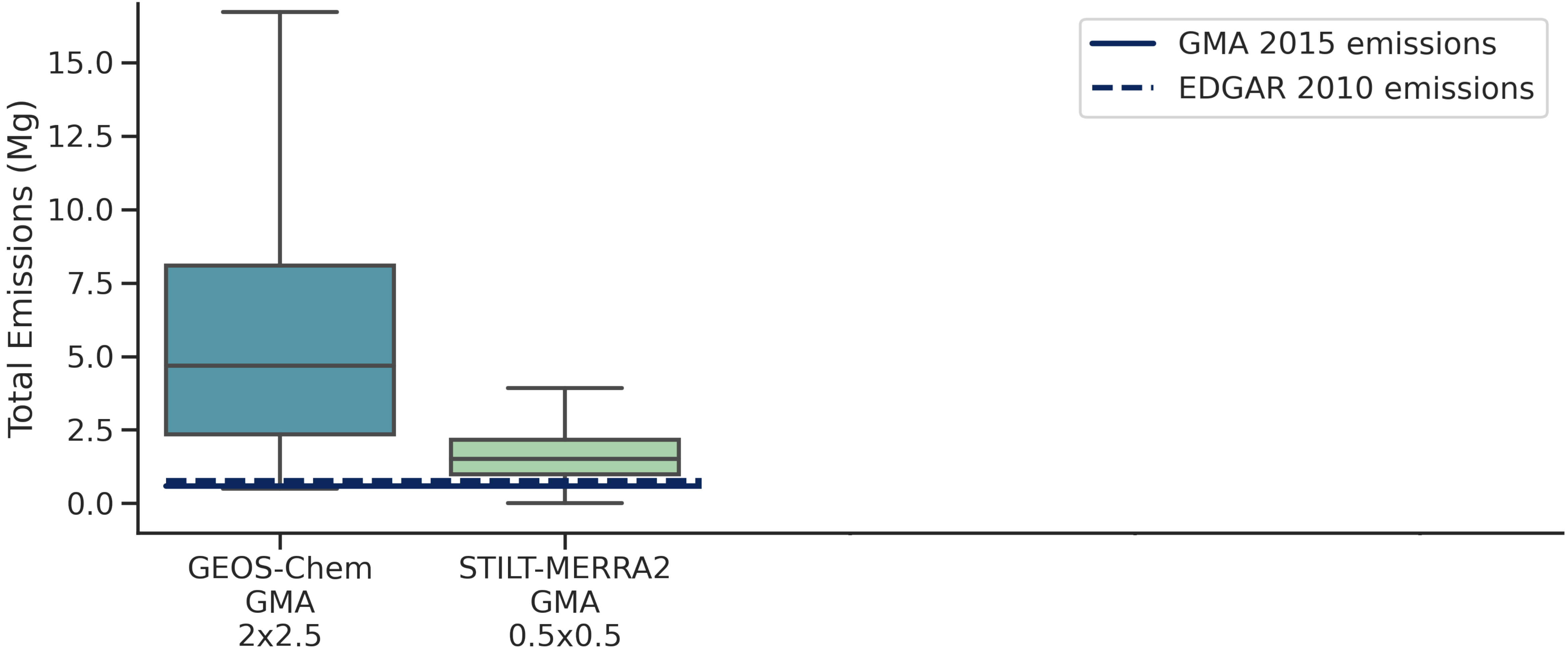

Optimized emissions in Madre de Dios

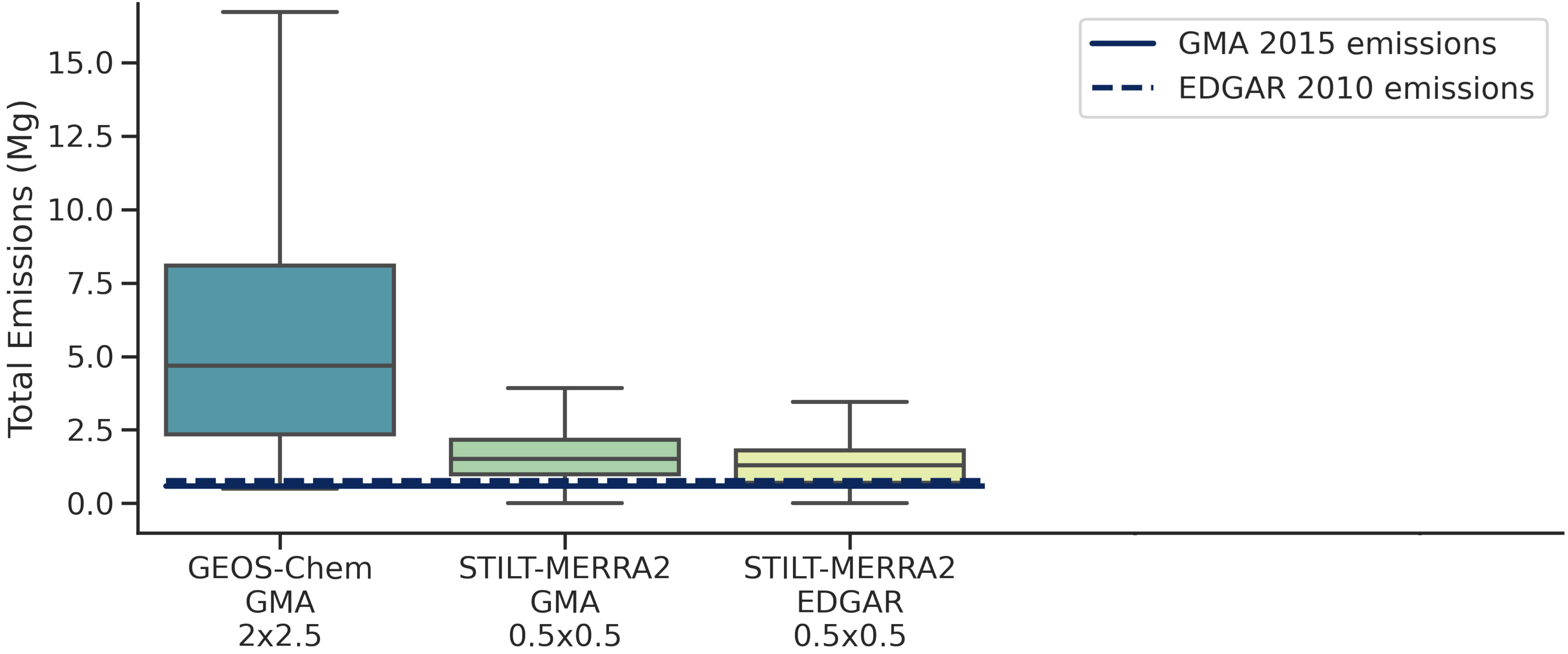

Optimized emissions in Madre de Dios

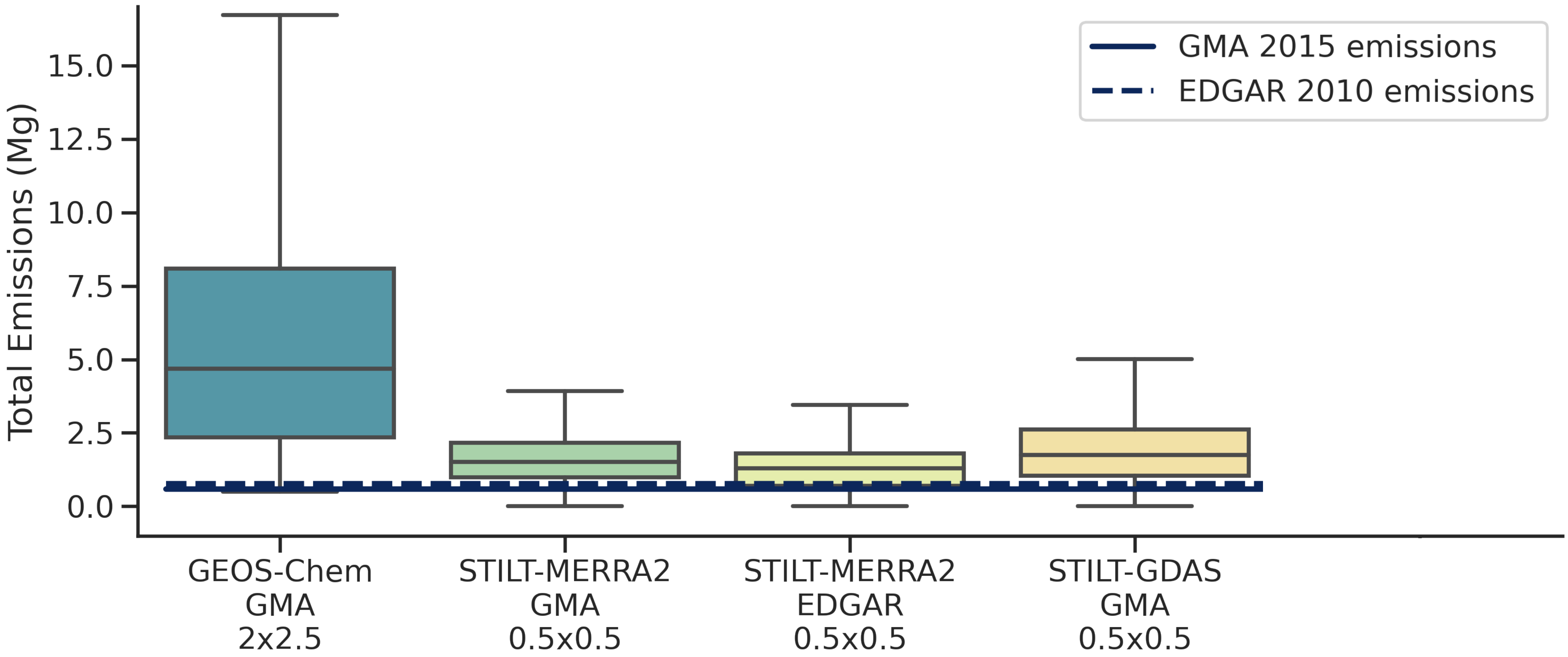

Optimized emissions in Madre de Dios

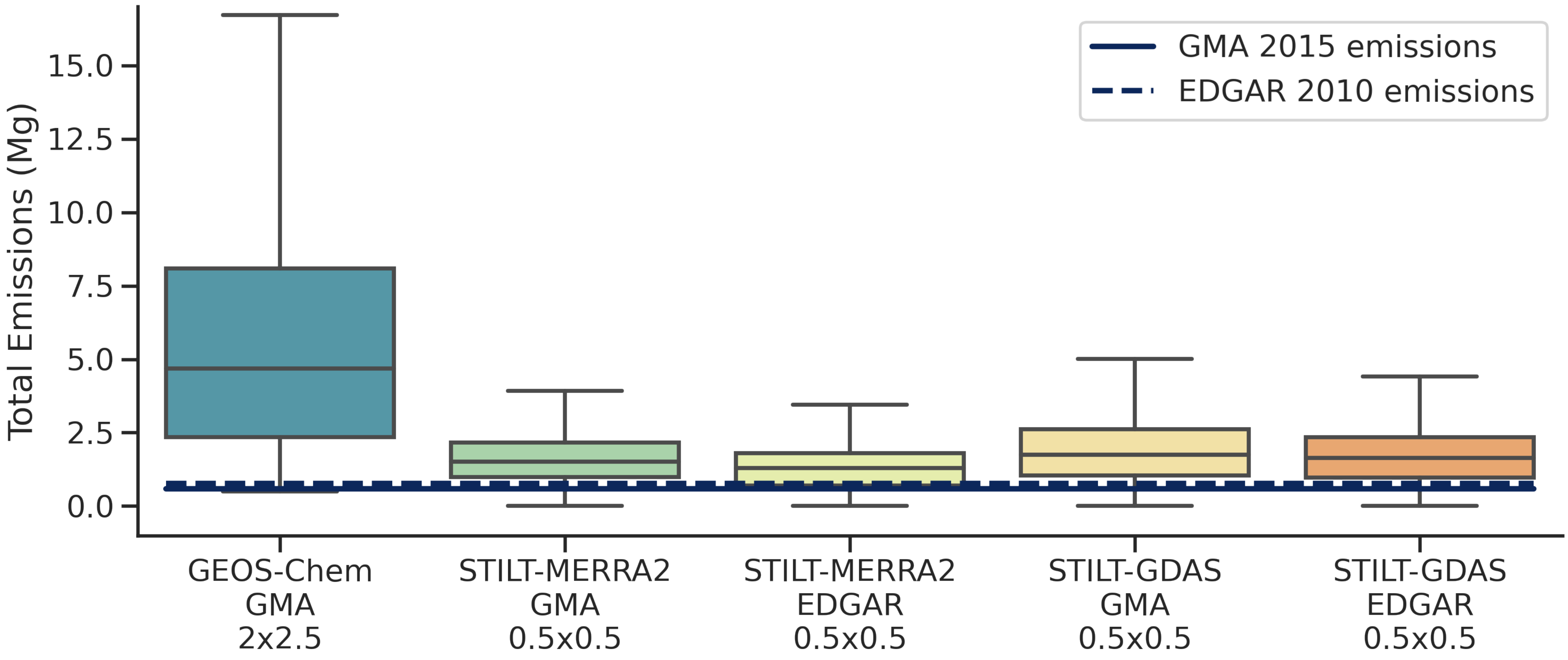

Optimized emissions in Madre de Dios

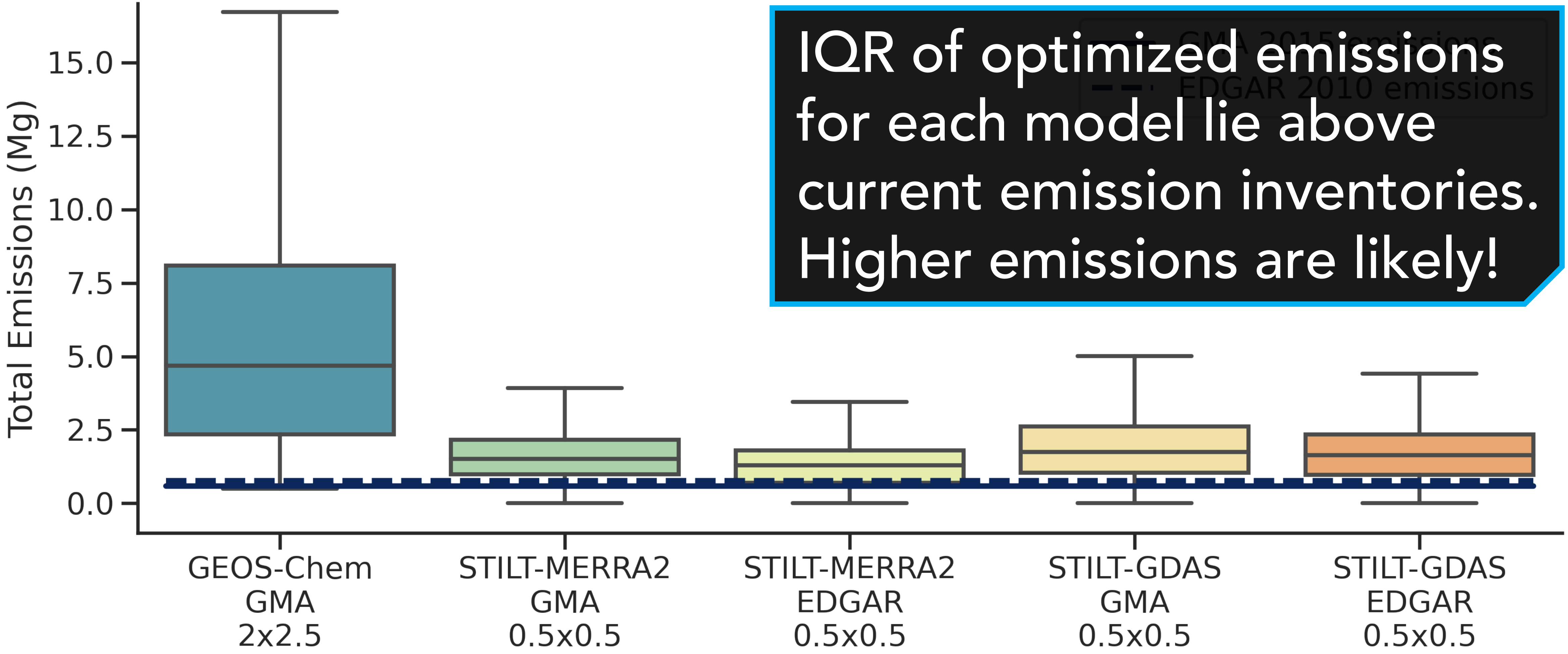

IQR of optimized emissions for each model lie above current emission inventories. Higher emissions are likely!

Gunn Point, AU concentration frequently sample savannah biomass burning plumes

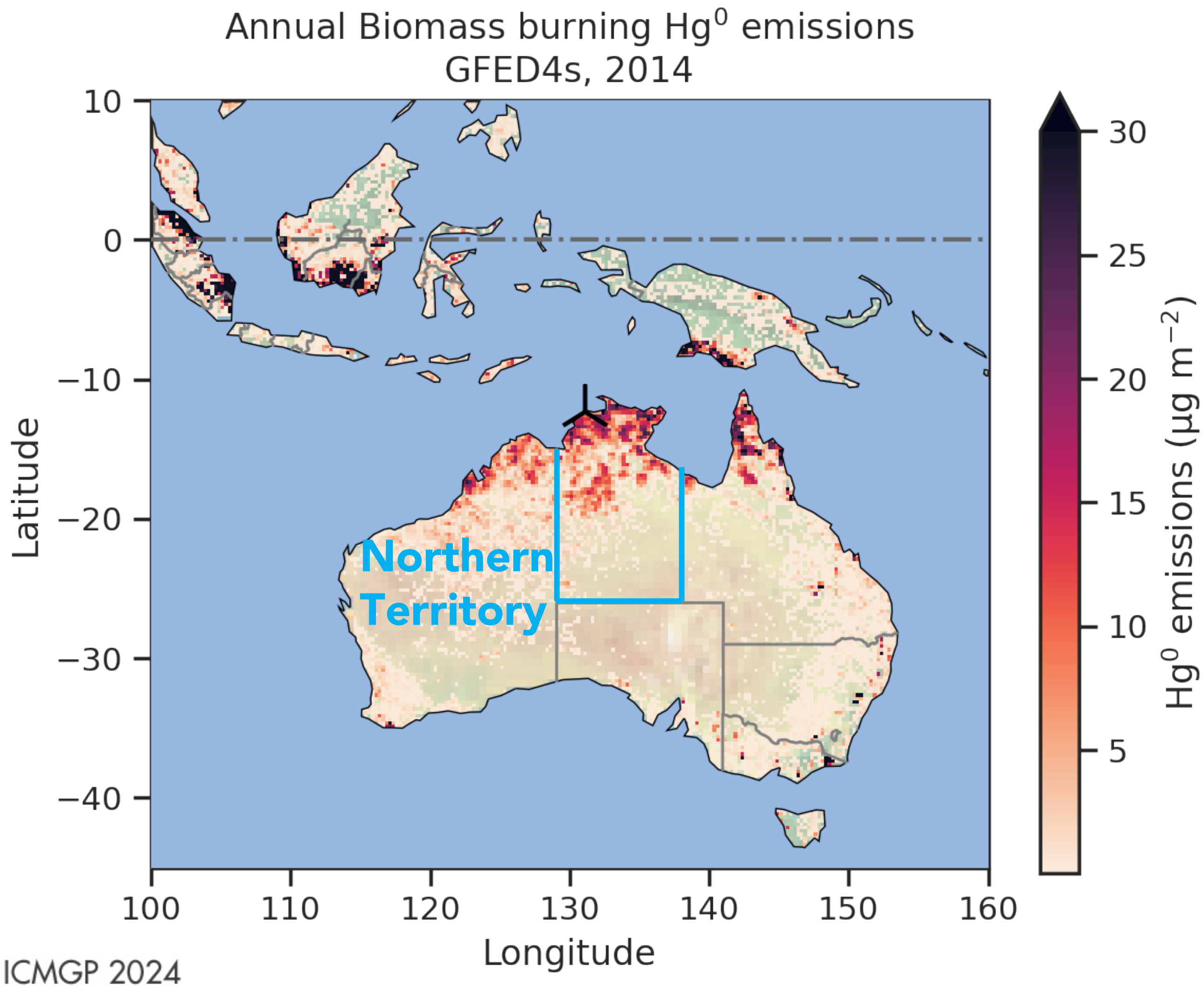

Gunn Point, AU concentration frequently sample savannah biomass burning plumes

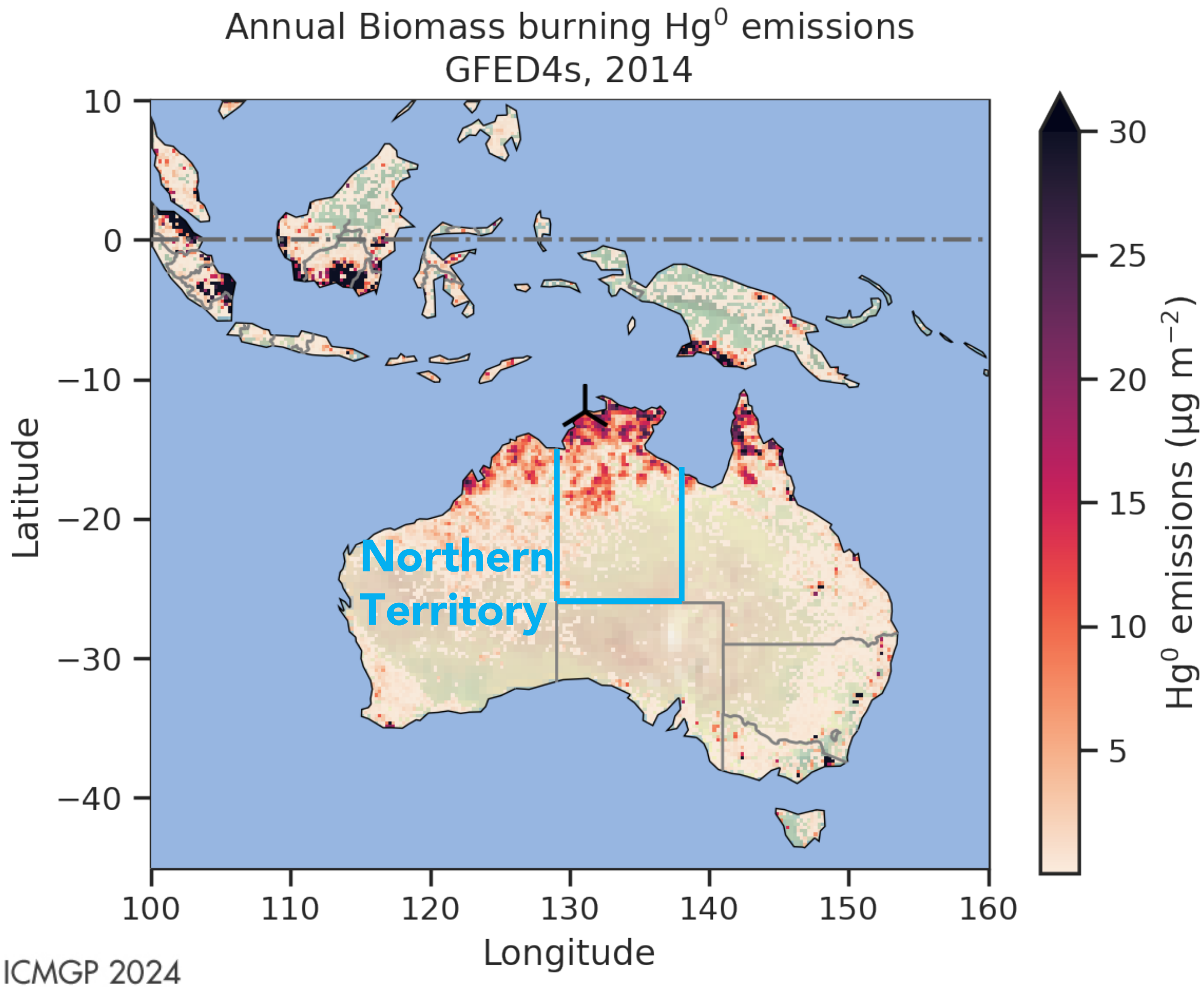

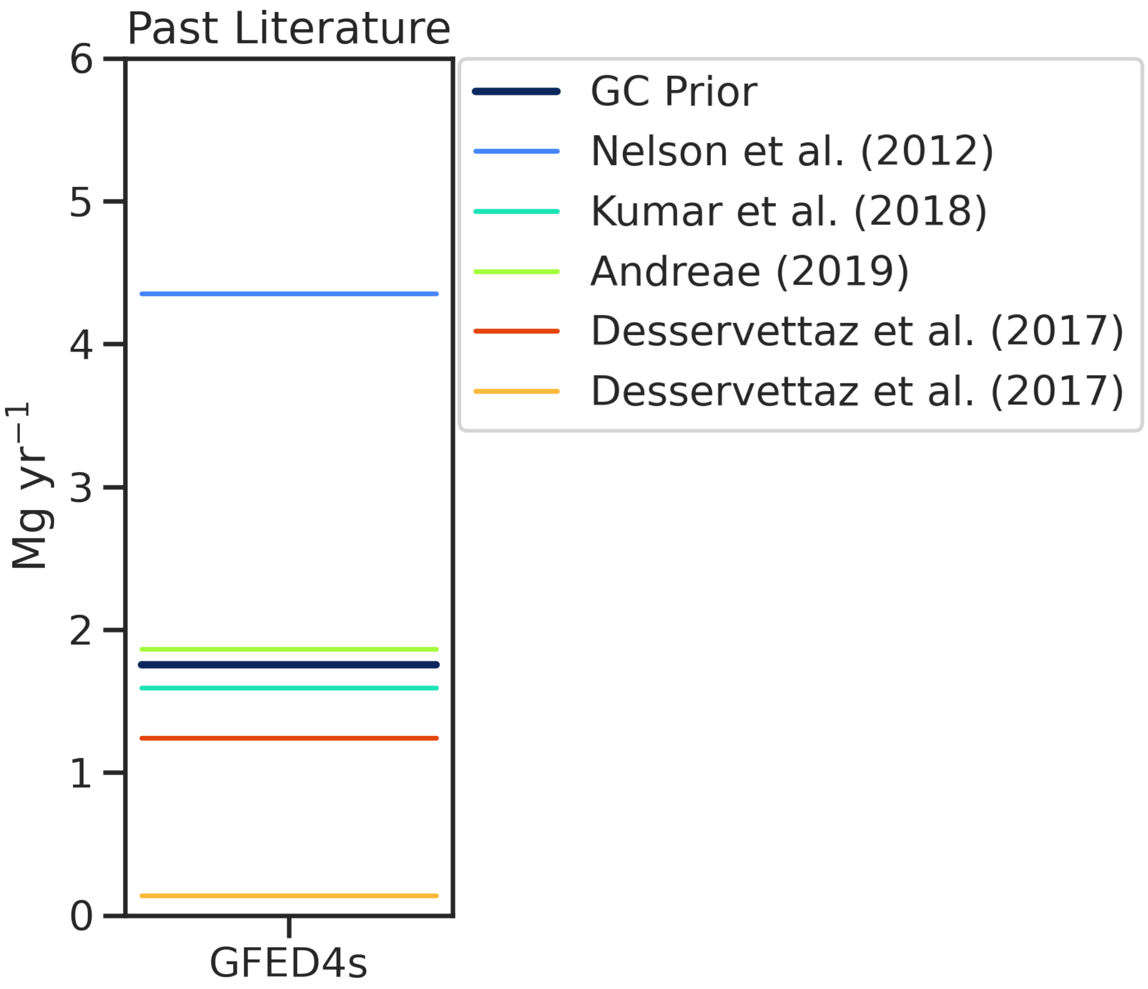

Gunn Point, AU concentration frequently sample savannah biomass burning plumes

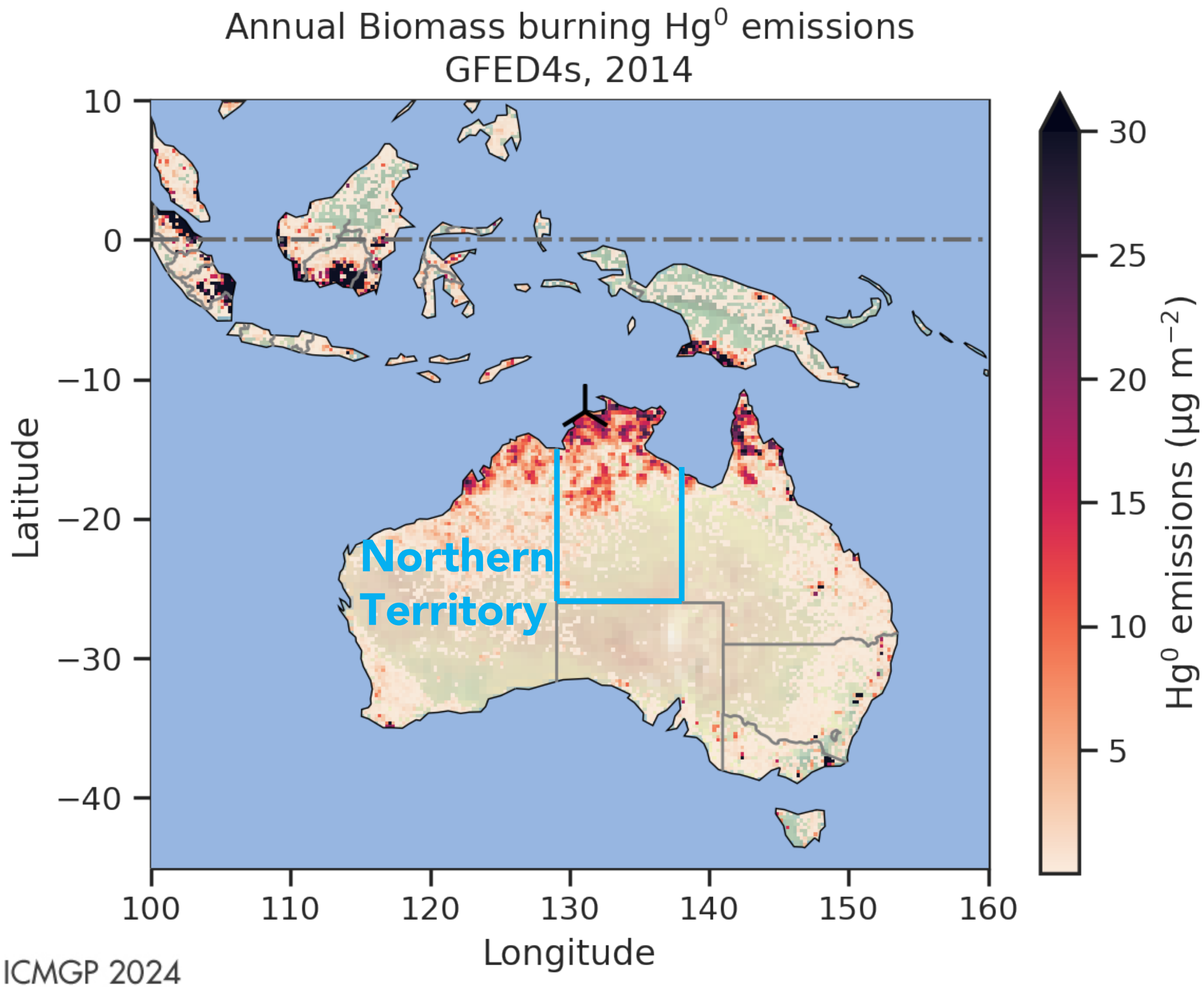

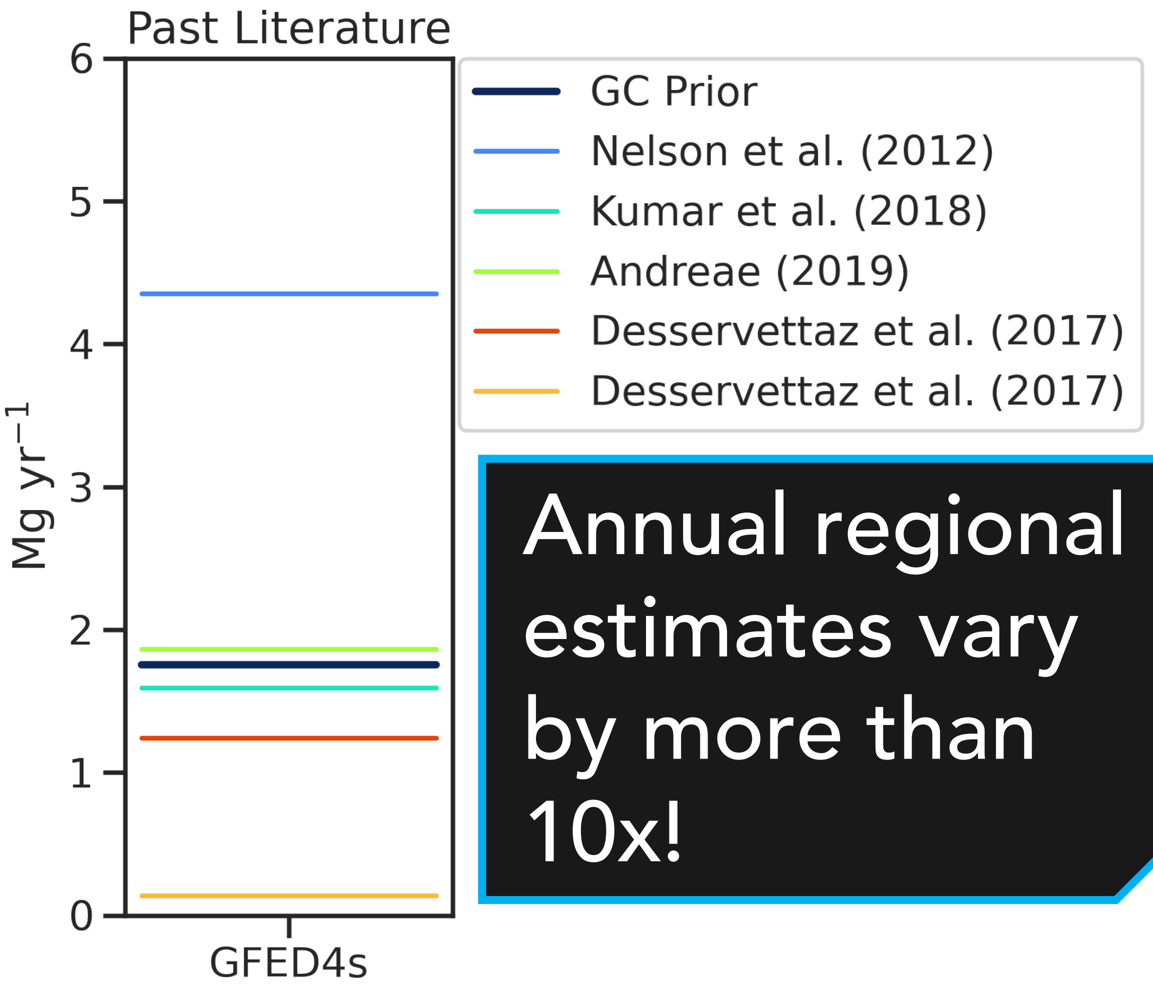

Annual regional estimates vary by more than 10x!

Optimized Biomass Burning Emissions

Optimized Biomass Burning Emissions

Optimized Biomass Burning Emissions

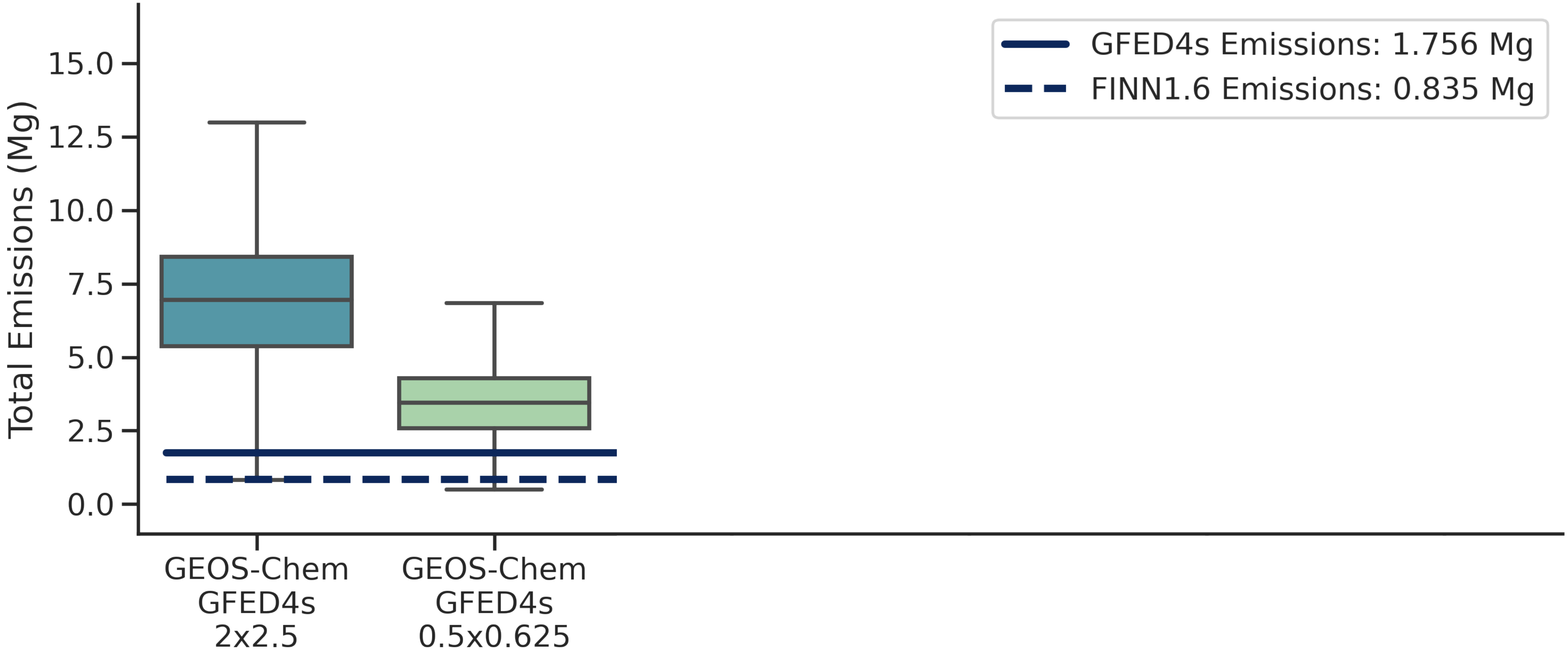

Optimized Biomass Burning Emissions

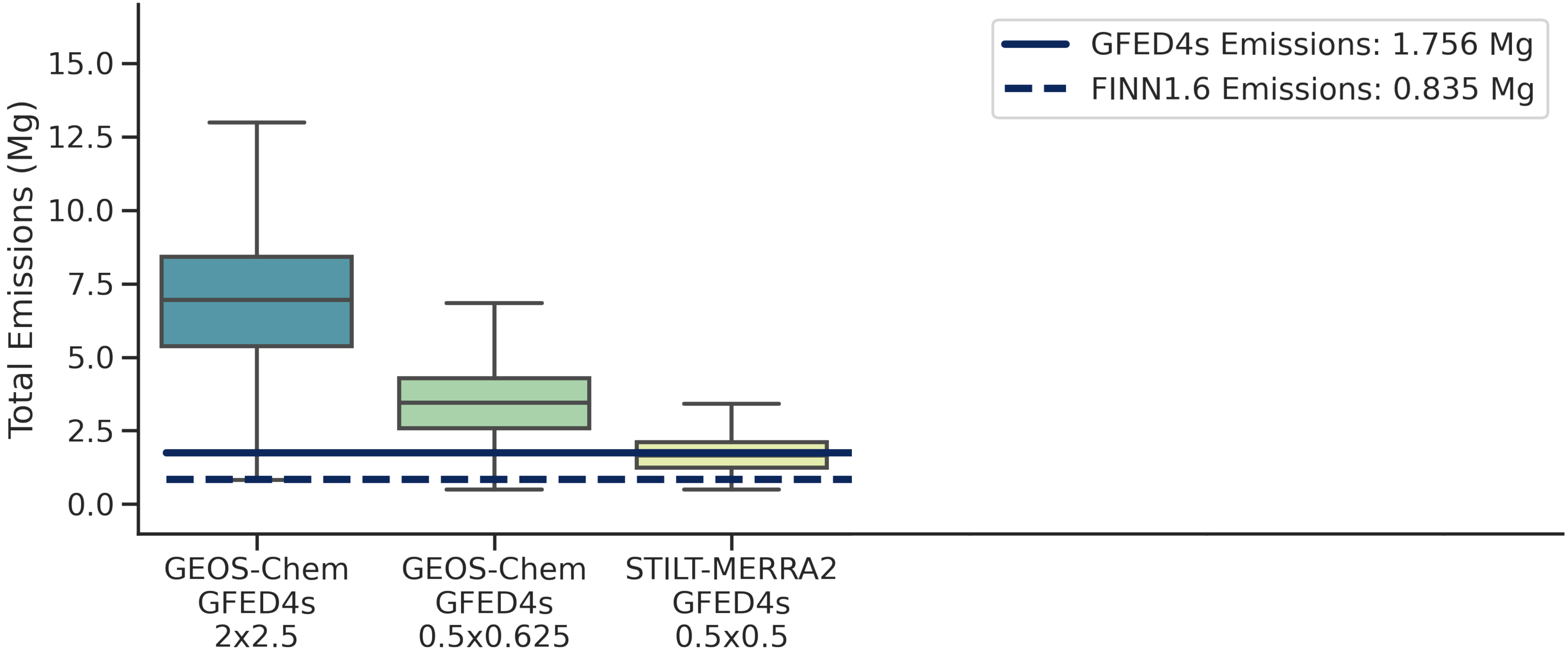

Optimized Biomass Burning Emissions

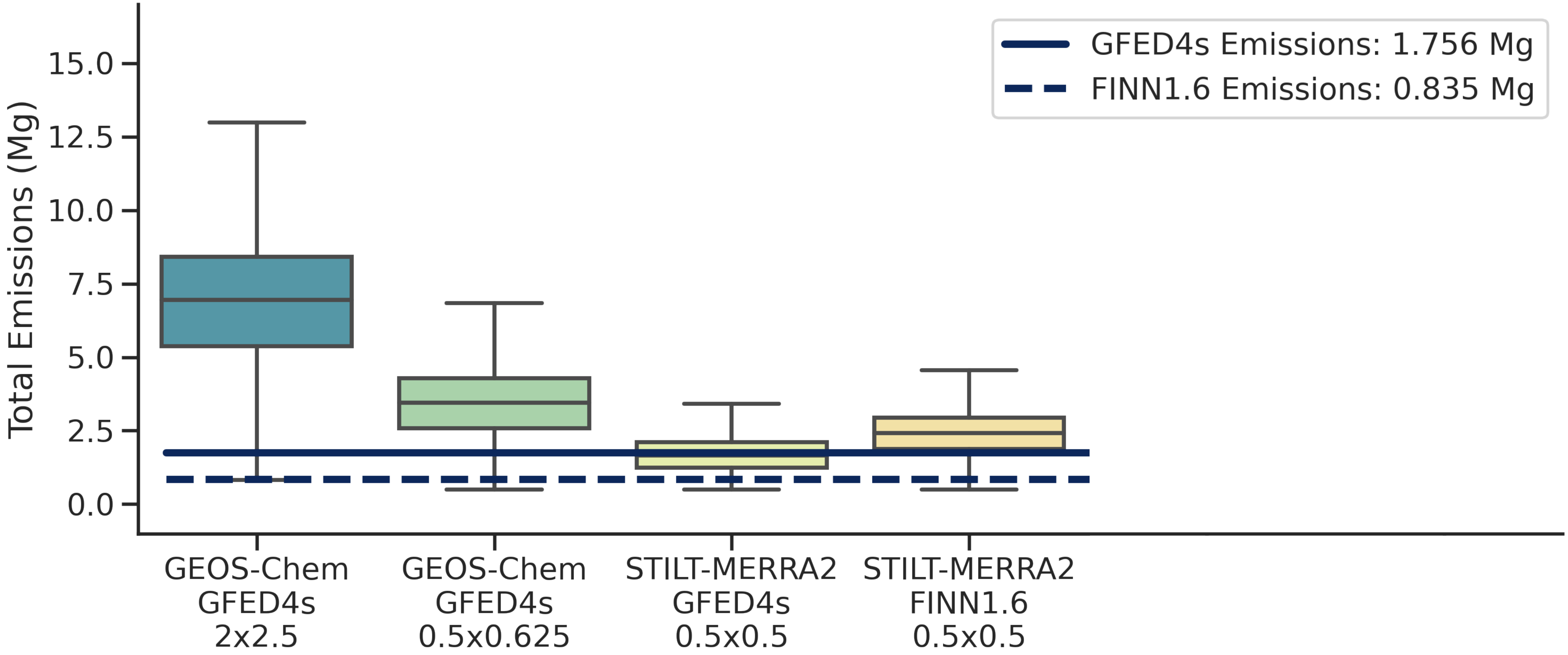

Optimized Biomass Burning Emissions

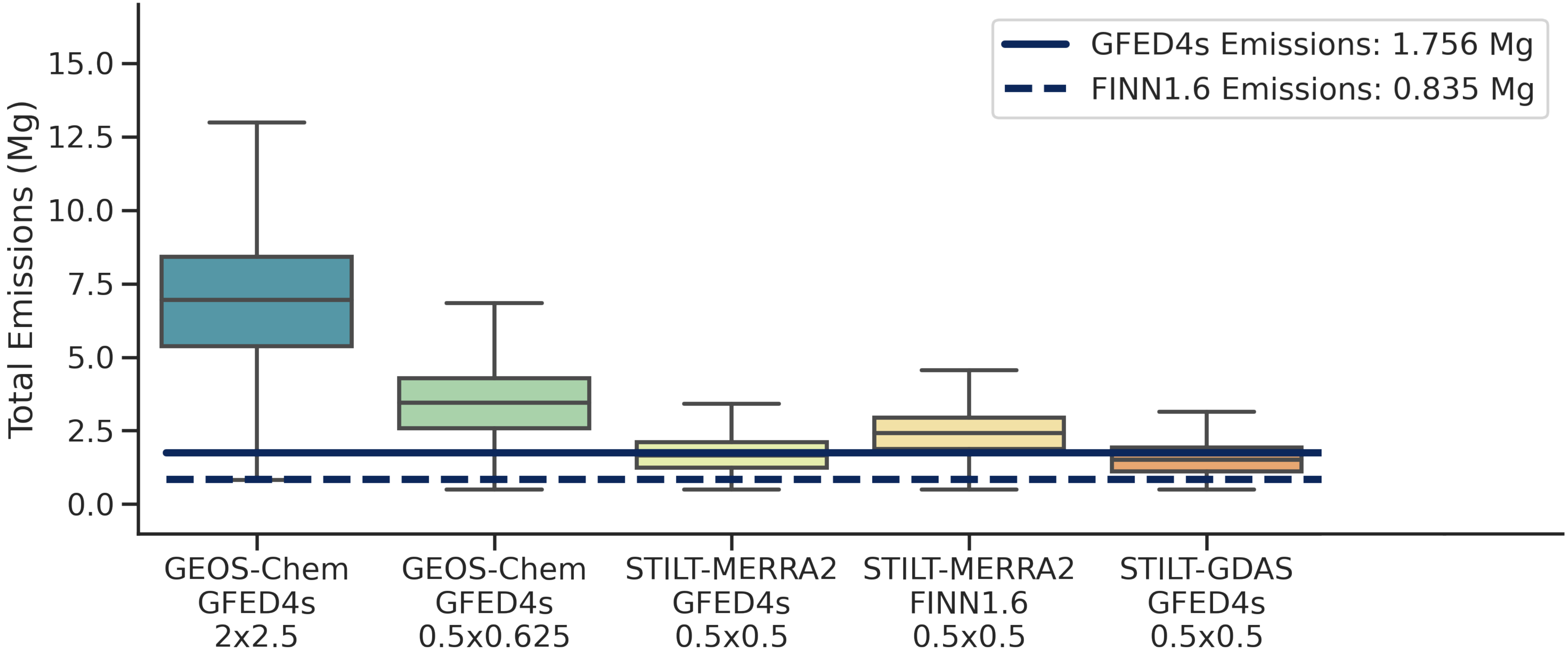

Optimized Biomass Burning Emissions

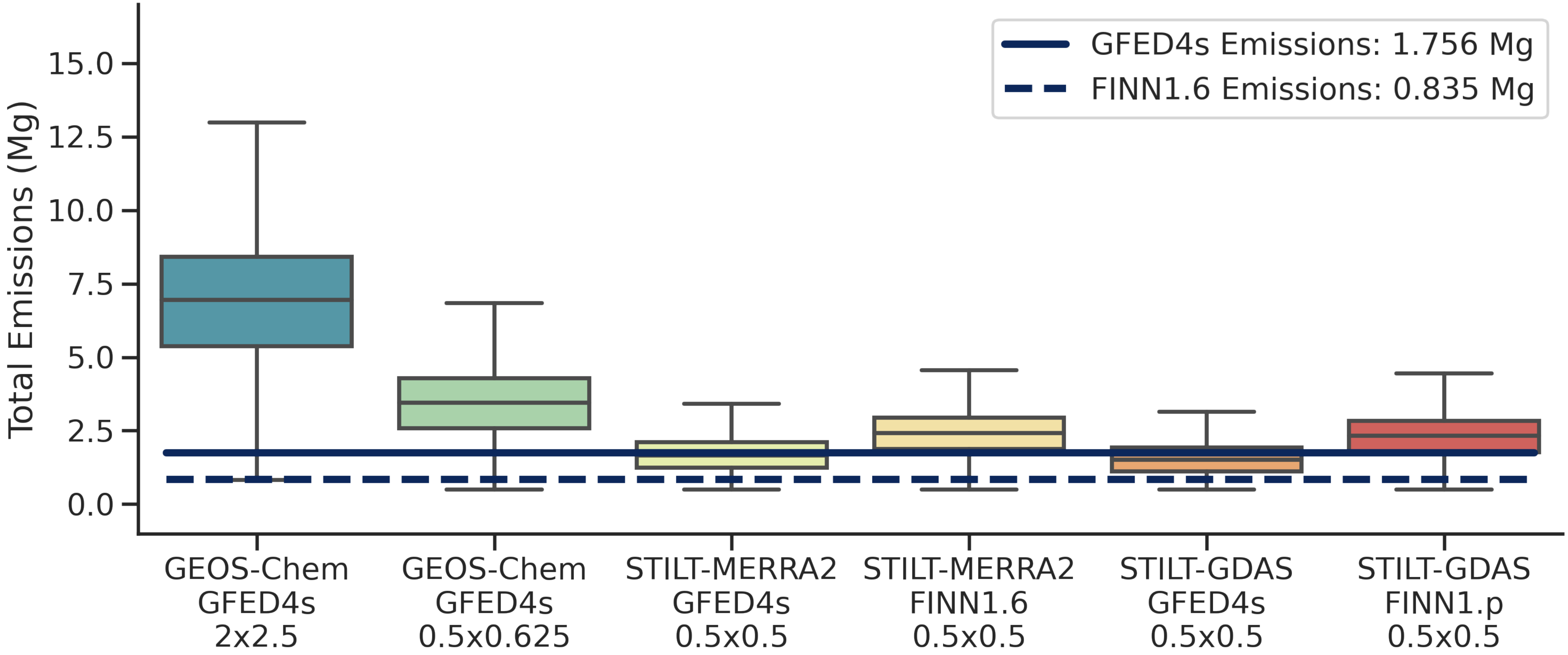

Optimized Biomass Burning Emissions

Existing estimates lie within range of optimized emissions for several models.

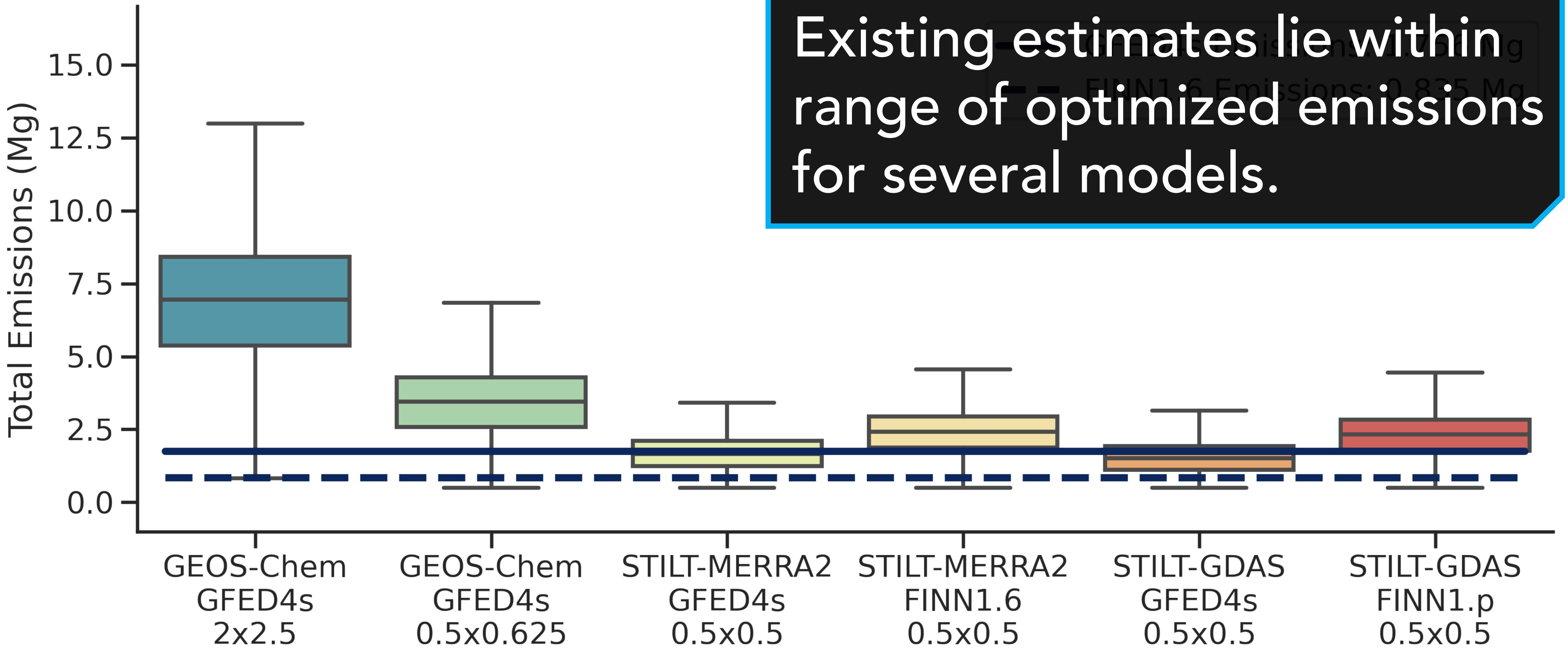

Optimized Biomass Burning Emissions

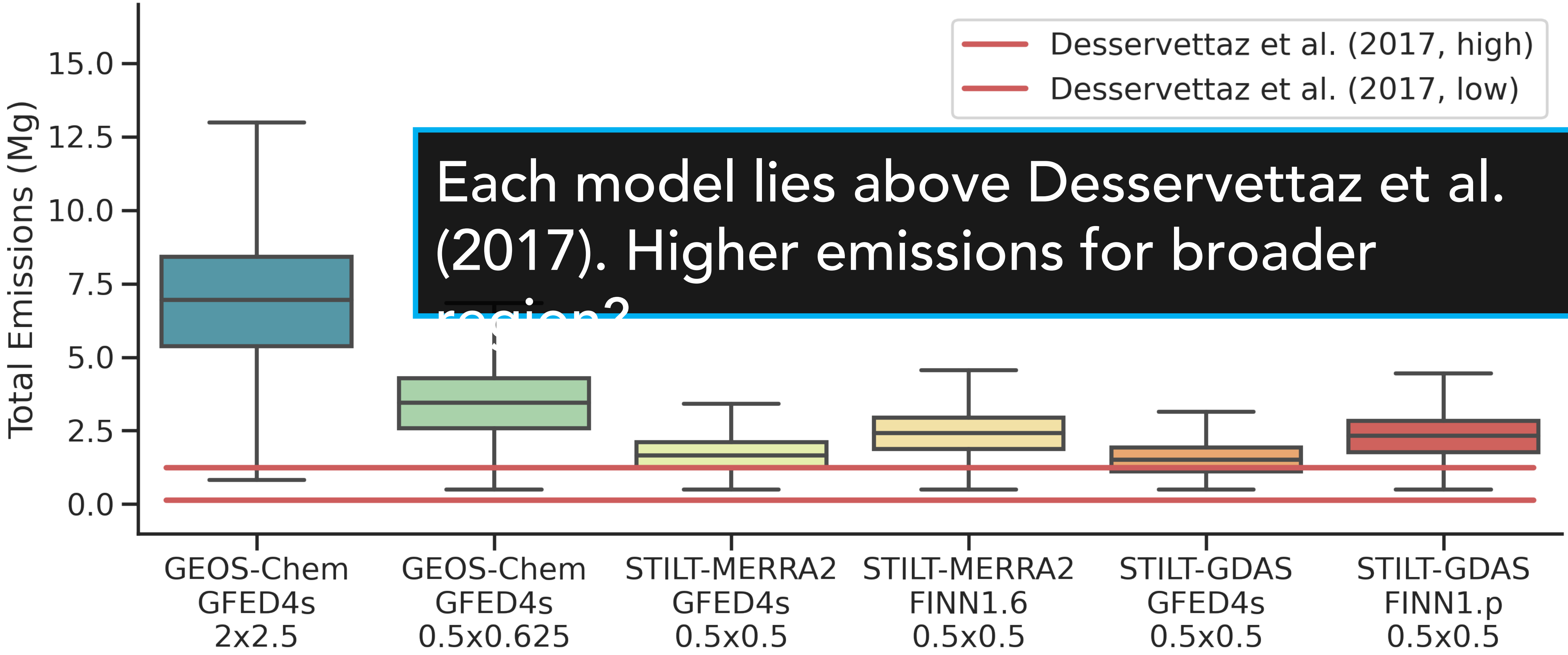

Each model lies above Desservettaz et al. (2017). Higher emissions for broader region?

Concluding remarks

- Demonstrate inverse modeling framework for top-down constraint of regional surface fluxes.
- Informative results rely on an adequate representation of uncertainty (e.g., measurement, meteorological, and structural errors).
- We extract additional value from already existing measurements, justifying the continued support of long-term monitoring stations.

Funding:
EAPS Callahan-Dee Fellowship, EAPS Houghton Endowment, MIT Presidential Fellowship, NSF Grant #1924148

Helpful conversations and additional guidance:
Ari Feinberg, Noelle Selin, Yuying Cui, Selin Group, Ed Boyle Andrew Babbin, and Tim Cronin

CSIC
CONSEJO SUPERIOR DE INVESTIGACIONES CIENTÍFICAS
UOW AUSTRALIA
CSIRO
NSF